Transcriptional and Cellular Response of hiPSC-derived Microglia-Neural Progenitor Co-Cultures Exposed to IL-6

Amalie C. M. Couch[1,2*], Amelia M. Brown[1,2], Catarina Raimundo[1,3], Shiden Solomon[1], Morgan Taylor[1], Laura Sichlinger[1,2], Rugile Matuleviciute[1,2], Deepak P. Srivastava[1,2§], Anthony C. Vernon[1,2*§].

1. Department of Basic and Clinical Neuroscience, Institute of Psychiatry, Psychology and Neuroscience, King's College London, London, UK.
2. MRC Centre for Neurodevelopmental Disorders, King's College London, London, UK.
3. Faculty of Life Sciences and Medicine, King's College London, London, UK.

§ These authors share joint senior authorship

***Joint Corresponding authors:**
Dr. Amalie Couch and Dr. Anthony Vernon
Department of Basic and Clinical Neuroscience
Maurice Wohl Clinical Neuroscience Institute
Institute of Psychiatry, Psychology and Neuroscience
King's College London
London SE5 9RT, United Kingdom

Tel: +44 (0) 207 848 5311
Email: anthony.vernon@kcl.ac.uk or amalie.c.couch@kcl.ac.uk

KEYWORDS
IL-6, neurodevelopment, human induced-pluripotent stem cells, microglia, neural progenitor cells.

Abstract

Elevated interleukin (IL-)6 levels during prenatal development have been linked to increased risk for neurodevelopmental disorders (NDD) in the offspring, but the mechanism remains unclear. Human-induced pluripotent stem cell (hiPSC) models offer a valuable tool to study the effects of IL-6 on features relevant for human neurodevelopment *in vitro*. We previously reported that hiPSC-derived microglia-like cells (MGLs) respond to IL-6, but neural progenitor cells (NPCs) in monoculture do not. Therefore, we investigated whether co-culturing hiPSC-derived MGLs with NPCs would trigger a cellular response to IL-6 stimulation via secreted factors from the MGLs. Using N=4 donor lines without psychiatric diagnosis, we first confirmed that NPCs can respond to IL-6 through trans-signalling when recombinant IL-6Ra is present, and that this response is dose-dependent. MGLs secreted soluble IL-6R, but at lower levels than found *in vivo* and below that needed to activate trans-signalling in NPCs. Whilst transcriptomic and secretome analysis confirmed that MGLs undergo substantial transcriptomic changes after IL-6 exposure and subsequently secrete a cytokine milieu, NPCs in co-culture with MGLs exhibited a minimal transcriptional response. Furthermore, there were no significant cell fate-acquisition changes when differentiated into post-mitotic cultures, nor alterations in synaptic densities in mature neurons. These findings highlight the need to investigate if trans-IL-6 signalling to NPCs is a relevant disease mechanism linking prenatal IL-6 exposure to increased risk for psychiatric disorders. Moreover, our findings underscore the importance of establishing more complex *in vitro* human models with diverse cell types, which may show cell-specific responses to microglia-released cytokines to fully understand how IL-6 exposure may influence human neurodevelopment.

Introduction

Human birth cohort studies have linked elevated maternal interleukin (IL)-6 concentrations across gestation with aberrant structural and functional brain connectivity in the offspring, as measured by MRI, which in turn are associated with abnormal cognitive development and increased risk for neurodevelopmental disorders (NDDs) such as autism spectrum condition (ASC) and schizophrenia (SZ) (Graham *et al.*, 2018; Rudolph *et al.*, 2018; Rasmussen *et al.*, 2019; Allswede *et al.*, 2020). Although these cohort studies demonstrate a correlation between elevated prenatal IL-6 and NDD incidence, additional studies at a molecular and cellular level are required to elucidate the molecular mechanisms by which this risk is conferred. Much of the cellular level research that links prenatal IL-6 insults with adverse neurodevelopmental effects in the offspring has, however, been conducted in rodent models (Samuelsson *et al.*, 2006; Smith *et al.*, 2007; Ozaki *et al.*, 2020; Mirabella *et al.*, 2021), which may have different brain development trajectories (Eze et al., 2021) For example, transient elevation of IL-6 during a critical period of neurodevelopment can have enduring effects on the formation of glutamatergic synapses in the mouse hippocampus with consequences for mouse brain connectivity as measured by resting state fMRI (Samuelsson *et al.*, 2006; Mirabella *et al.*, 2021). Nonetheless, investigating the influence of IL-6 on early neurodevelopmental processes using human-led models is crucial to understand its role in increasing the risk of NDDs in offspring (Bayés *et al.*, 2011; Südhof, 2017; Kuljis *et al.*, 2019).

As previously reviewed, IL-6 signalling involves both the IL-6 receptor (IL-6Ra) and IL-6 signal transducer (IL-6ST) subunits, with IL-6 binding to IL-6Ra triggering a conformational change that activates the JAK/STAT pathway through either cis-

50 signalling (cell surface IL-6Ra expression) or trans-signalling (via secreted soluble IL-
51 6Ra, sIL-6Ra) (Rose-John, 2001, 2012, 2018; Wolf, Rose-John and Garbers, 2014).
52 Trans-signalling via sIL-6Ra enables activation of cells lacking the full receptor and
53 may be implicated in pro-inflammatory effects on non-glial cells, contrasting cis-
54 signalling's proposed anti-inflammatory effects (Rose-John, 2001, 2012; Rose-John
55 *et al.*, 2009; Scheller *et al.*, 2011; Campbell *et al.*, 2014; Wolf, Rose-John and Garbers,
56 2014). This mechanism is known to occur in the CNS, demonstrated when blocking
57 trans-signalling with soluble IL-6ST in the CNS of adult rodents, which resulted in
58 reduced astrogliosis and microgliosis, blood-brain barrier leakage, vascular
59 proliferation, neurodegeneration, as well as impaired neurogenesis, caused by
60 overexpression of IL-6 (Campbell *et al.*, 2014). However, the consequences of trans-
61 IL-6 signalling during human development remains unclear.

62

63 Microglia are central to the developing brain's response to IL-6. In mid-gestation
64 (GW17-18) human neocortex tissue (Polioudakis *et al.*, 2019), as well as in the
65 developing human telencephalon (Florio *et al.*, 2015; Zhang *et al.*, 2016; Nowakowski
66 *et al.*, 2017), microglia are the leading cell type expressing IL-6Ra, with expression
67 levels being higher than in excitatory neurons, intermediate progenitors, interneurons,
68 radial glia, mitotic progenitors, oligodendrocyte precursors, endothelial cells and
69 pericytes. Importantly, initiation of either IL-6 trans- or cis- signalling may be
70 dependent on the expression ratios of the receptor complex's subunits (Reeh *et al.*,
71 2019). However, the direct link between sIL-6Ra secretion by microglia and enhanced
72 trans-signalling in non-glial cells (Ferreira *et al.*, 2013; Campbell *et al.*, 2014), as well
73 as its implications in a neurodevelopment system remain uncertain, especially in a
74 human-relevant model. This knowledge gap underscores the value of using human-

75 induced pluripotent stem cells (hiPSCs) to model human foetal brain development
76 (Eze *et al.*, 2021). In agreement with primary tissue studies (Florio *et al.*, 2015; Zhang
77 *et al.*, 2016; Nowakowski *et al.*, 2017; Polioudakis *et al.*, 2019), hiPSC-derived NPCs
78 express IL-6ST, yet they lack IL-6Ra expression (Couch *et al.*, 2023; Sarieva,
79 Hildebrand, *et al.*, 2023). This renders them unresponsive to IL-6 in mono-culture
80 without the addition of sIL-6Ra necessary for trans-signalling (Couch *et al.*, 2023;
81 Sarieva, Hildebrand, *et al.*, 2023). To circumvent this limitation, previous *in vitro*
82 studies by using hyper-IL-6, a synthetic construct combining sIL-6Ra and IL-6 linked
83 by a flexible peptide, enabling NPCs to respond to IL-6 through trans-signalling
84 (Sarieva, Hildebrand, *et al.*, 2023). Recent investigations using a 3D human forebrain
85 organoid, which lacked microglia, demonstrated that exposure to hyper-IL-6
86 disproportionately affected radial glia cells, leading to an increased presence of this
87 cell type in the organoid (Sarieva, Kagermeier, *et al.*, 2023). Notably, chronic 5-day
88 hyper-IL-6 exposure also resulted in an increase in upper-layer excitatory neurons and
89 abnormalities in neuronal migration and positioning, suggesting that forced IL-6 trans-
90 signalling can disrupt the standard process of cortical development and organisation
91 (Sarieva, Kagermeier, *et al.*, 2023). These data provide human-relevant evidence that
92 IL-6 signalling in developing forebrain organoids can change typical cellular and
93 molecular phenotypes.

94

95 Although hyper-IL-6 effectively demonstrates that NPCs are capable of IL-6 trans-
96 signalling, it does not replicate the hypothesised physiological trans-signalling process
97 found *in vivo.* Hyper-IL-6 forces cells to respond via trans-signalling under any
98 condition, despite the fact there could be an upstream signalling regulation mechanism
99 governed by non-NPC cell types. Our previous research indicates that hiPSC-derived

100 microglia-like cells (MGLs) can secrete sIL-6Ra, addressing the absence of this
101 subunit in hiPSC-derived NPCs (Couch *et al.*, 2023). Consequently, a co-culture
102 system of MGLs and developing cortical NPCs may offer a more physiologically
103 relevant model to study the acute IL-6 responses of both cell types, providing a closer
104 approximation to physiological conditions than hyper-IL-6. In this study, we employ
105 hiPSC-derived MGLs and NPCs from the same donors for co-culture, ensuring a
106 consistent genetic background within each culture, and expose them to acute IL-6
107 stimulation for 24 hours. Employing a trans-well co-culture system allows for the
108 analysis of soluble factors, minimises potential confounding impact from the
109 experimental handling of microglia (Cadiz *et al.*, 2022), and precludes the need for
110 more invasive separation methods like fluorescence-activated cell sorting (FACS)
111 (Park *et al.*, 2020). The overall study aim was to ascertain the cellular and molecular
112 changes of both NPCs and MGLs post-IL-6 exposure. We hypothesised that: (1) co-
113 culturing with MGLs will facilitate acute NPC response to IL-6 via trans-signalling
114 mediated by sIL-6Ra, or additional cytokines secreted by MGLs in response to IL-6;
115 (2) this interaction will modify the transcriptomes of both MGLs and NPCs, as identified
116 through bulk RNAseq, revealing key molecular pathways; (3) early exposure of NPCs
117 to cytokines will influence their cell fate determination and synaptogenesis upon
118 differentiation into post-mitotic cortical neurons.

119 Methods

120 *Cell Culture*

121 **hiPSCs:** For the derivation of human induced pluripotent stem cells (hiPSCs),
122 participants were recruited, and methods carried out in accordance with the 'Patient
123 iPSCs for Neurodevelopmental Disorders (PiNDs) study' (REC No 13/LO/1218).

124 Informed consent was obtained from all subjects for participation in the PiNDs study.
125 Ethical approval for the PiNDs study was provided by the NHS Research Ethics
126 Committee at the South London and Maudsley (SLaM) NHS R&D Office. Human
127 iPSCs were generated from a total of four lines donated by three males and one female
128 with no history of neurodevelopmental or psychiatric disorders (Supplementary Table
129 1). All hiPSC donor lines used in this study have been previously characterised, as
130 described elsewhere (Warre-Cornish *et al.*, 2020; Adhya *et al.*, 2021; Pantazis *et al.*,
131 2022; Couch *et al.*, 2023). As such and following the International Society for Stem
132 Cell Research (ISSCR) standards for previously published lines, we performed
133 karyotyping and confirmed the expression of pluripotency markers (Supplementary
134 Figure 1). The cells were grown in hypoxic conditions on Geltrex™ (Life Technologies;
135 A1413302) coated 6-well NUNC™ plates in StemFlex medium (Gibco, A3349401)
136 exchanged every 48 hours. For passaging, cells were washed with HBSS (Invitrogen;
137 14170146) and then passaged by incubation with Versene (Lonza; BE17-711E), then
138 plated in fresh StemFlex onto fresh Geltrex-coated 6-well NUNC™ plates.

139

140 **Microglia-like and Neural Progenitor Cell Co-culture:** Microglia-like cells (MGL)
141 differentiation from hiPSCs was performed following a previously published protocol
142 (van Wilgenburg *et al.*, 2013; Haenseler *et al.*, 2017), and successfully replicated by
143 our group (Couch *et al.*, 2023). Simultaneously but in separate cultures, hiPSCs from
144 the same lines were neuralised towards neural progenitor cells (NPCs) using a
145 modified dual SMAD inhibition protocol to develop a mixture of excitatory and inhibitory
146 forebrain neuronal subtypes (Shi, Kirwan and Livesey, 2012; Warre-Cornish *et al.*,
147 2020; Adhya *et al.*, 2021; Bhat *et al.*, 2022; Couch *et al.*, 2023), and were characterised
148 for Nestin and β-tubulin III (TUBB3, antibody name TUJ1) expression using

149 immunocytochemistry (Supplementary Figure 2). MGL progenitors were seeded
150 directly from the embryoid body factory onto 0.4 µm Transparent PET Membrane
151 Permeable Support Cell Culture Inserts (Falcon®; 353090) and allowed to differentiate
152 for 12 days, after which they were assembled on top of the NPCs that had been
153 differentiating in parallel for 16 days (Supplementary Figure 3). This permitted the
154 NPCs to settle after neural passaging the day before on day 15 of their differentiation.
155 Both cell types were then cultured together for 48h in co-culture media (1X N2
156 supplement, 2mM Glutamax, 100ng/ml IL-34 and 10ng/ml GM-CSF), to allow the two
157 cell types to "equilibrate". Specifically, during their initial optimization trials for
158 establishing the hiPSC to MGL differentiation method, Haenseler *et al.* (2017) raised
159 concerns regarding the presence of corticosterone, superoxide dismutase, and
160 catalase compounds in the B27 supplement. Therefore, B27 was removed from co-
161 culture medium to guarantee compatibility with iPSC-derived cortical neurons while
162 preserving microglial function (Haenseler *et al.*, 2017). The co-cultures were then
163 exposed to 100ng/ml IL-6 or vehicle control (sterile water with 100 pM acetic acid) in
164 fresh media, for 24h (Supplementary Figure 3). This meant stimulation on the
165 microglial differentiation day 14, and neural progenitor differentiation day 18 (Couch
166 *et al.*, 2023). The differentiation timepoints and 100ng/ml IL-6 dosage were based on
167 previously published data that examined the IL-6 dose-response in day 14 MGLs
168 (Couch *et al.*, 2023). After 24h of IL-6 or vehicle exposure, MGLs and NPCs were
169 reseparated. All MGLs were collected for RNAseq, half NPCs were collected for
170 RNAseq, and half were terminally differentiated into post-mitotic neurons as follows
171 (Supplementary Figure 3).

172

173 **Post-mitotic Cortical Neuron Differentiation:** After 24h of IL-6 stimulation in co-
174 culture with MGLs, half the NPCs were subsequently terminally differentiated into post-
175 mitotic cortical neurons. NPCs to be terminally differentiated were passaged three
176 days after IL-6 stimulation (D21) into 50ng/ml poly-l-ornithine (Gibco; A3890401) and
177 20ng/ml laminin (Sigma; L2020) coated 96-well Perkin Elmer CellCarrier Ultra plates,
178 at a density of 30,000 cells/well in 1X B27 + 10μM DAPT + 10μM Rock inhibitor and
179 incubated (37°C; 5% CO_2; 20% O_2). After 24 hours, medium was replaced with Rock
180 inhibitor-free medium every 24 hours until D28. After this time frame, the notch inhibitor
181 DAPT was removed from the medium and cells were fed with half 1X B27 medium
182 exchanges every 7 days.

183

184 ***Immunoblotting***

185 Protein samples were collected by scraping in ice cold RIPA Lysis and Extraction
186 Buffer (Thermo Scientific; 89900), with Phosphatase Inhibitor Cocktail 3 (1:100 Sigma;
187 P0044), AEBSF (1 mM), Leupeptin (10 μg/ml) and Aprotinin (10 μg/ml). Cells were
188 then lysed by sonication at 40% for 10 pulses, then centrifuged to pellet out insoluble
189 materials at 20,000 x *g* for 15 min at 4 ºC, with proteins collected in the supernatant.
190 Protein concentration was quantified using the Pierce™ BCA protein assay kit
191 (Thermo-Fisher; 23227). In preparation for SDS-PAGE separation, protein samples
192 were denatured in 2x Laemmli Sample Buffer (BioRad; 1610737EDU) with 5% 2-
193 Mercaptoethanol and boiled at 95ºC for 5min. 2 μg of each protein sample was loaded
194 into 10% acrylamide gels, alongside 5 μl of the Dual Color (BioRad;1610374) standard
195 marker. Gels were run at 20mA for approximately 20 min, then increased to 100V until
196 the samples reached the bottom of the unit (~90min). Separated samples were

197 transferred to a PVDF membrane and run overnight at 78mA at 4ºC. Blots were
198 blocked in 5% BSA TBS-T for 1 hour at RT with agitation. Antibodies (pSTAT3-Y705
199 Cell Signalling #9138S, total-STAT3 Cell Signalling #30835S, Phospho-p44/42 MAPK
200 (pERK1/2-T202/Y204) Cell Signalling #9101, p44/p42 MAPK (total ERK1/2) Cell
201 Signalling #4696S, GAPDH abcam #ab9484 and Beta-Actin Invitrogen #MA5-15739)
202 were diluted in blocking buffer; primary antibody incubation occurred overnight at 4ºC
203 with agitation, and secondary antibody incubation at RT for 1 hour with agitation.
204 Washes between antibody probes occurred in TBS-T at three 15min intervals. For
205 visualization, ECL Western Blotting Substrate (GE Healthcare; RPN2106) was
206 incubated on the blot at RT for 5min before image capture by the Bio-Rad Molecular
207 Imager® Gel Doc™ XR System. Blots were probed with antibodies directed towards
208 the phosphorylated protein first, then total protein and finally the loading control beta-
209 actin or GAPDH. Blots were stripped between each staining session by incubating the
210 membrane in Restore™ Stripping Buffer (Thermo Fischer Scientific; 21059) for 20mins
211 at RT, then rinsing with TBS-T three times before moving onto re-blocking with 5%
212 BSA TBS-T to commence the next probing phase. Blot signals were quantified using
213 ImageStudioLite (LI-COR, version 5.2.5), by defining an identical rectangular region
214 of interest around each signal band and measuring the median signal value.
215 Background correction was then performed using the automatic background detection
216 toolkit provided with the aforementioned software. All target protein signals were
217 normalized to beta-actin signal. Then, data for the phosphorylated proteins (pSTAT3
218 or pERK1/2) was divided by the total protein (tSTAT3 or tERK1/2) signal data within
219 each lane, to give a ratio for each sample. Full length, uncropped blots are presented
220 in Supplementary Figures 6 and 7.

221

222 ***sIL6Ra ELISA***

223 The IL-6 Receptor (Soluble) Human ELISA Kit (Invitrogen; BMS214) was used to
224 quantify soluble IL-6Ra expression in cell culture media, following the manufacturer's
225 instructions. For the co-culture assay (Figure 2A), media from N=4 donor lines
226 (014_CTM, 127_CTM, M3_CTR and 069_CTF) were used. For the MGL monoculture
227 assay to measure sIL-6Ra at timepoints through to 48h (Figure 2B), cells from the
228 KOLF2.1J reference line (N=3 biological replicates from three distinct hiPSC-derived
229 myeloid factories) were stimulated with acetic acid vehicle or 100ng/ml IL-6. Media
230 was then collected after 0h (immediately after stimulation), 3h, 6h, 12h, 24h and 48h.
231 Collected media was used undiluted and measured in duplicate on the ELISA plate to
232 provide technical replicates. The optical density (OD) of the microwells was blanked
233 and measured at 450nm, and referenced against 620nm. The sIL6Ra concentration
234 was estimated against a seven-point reference curve as per the manufacturer's
235 instructions.

236

237 ***Cytokine Profiler***

238 Media was taken from cells in co-culture and immediately spun at 300 x *g* for 2 minutes
239 to remove cells and cellular debris from the supernatant, which was transferred to a
240 new tube, snap frozen and stored at -80ºC until use. Co-culture media samples were
241 grouped and pooled by treatment condition, leaving two membranes to be stained with
242 either vehicle or IL-6 treated culture supernatant. Cytokine profiling was carried out
243 following the manufactures instructions using the Proteome Profiler Human XL
244 Cytokine Array Kit **(**R&D Systems; ARY022B). The kit contained membranes with dots
245 of 105 different immobilised cytokine antibodies dotted with two technical replicates
246 each (Supplementary Figure 4). Each membrane was imaged for 10 minutes using

247 the Bio-Rad Molecular Imager® Gel Doc™ XR System. Dot blot signals were
248 quantified using the Protein Array Analyzer Palette plug-in for ImageJ, and technical
249 dot replicates averaged to one value. These values were then corrected for
250 background staining by subtracting the mean negative reference value from each of
251 the signals. Each corrected value was then normalised by dividing by the mean
252 positive reference value on the membrane.

253

254 ***Custom Meso Scale Discovery Cytokine Array***

255 Based on the previous cytokine profiler analysis, the concentrations of MIP-1a, TNF-
256 α, IL-8, and VEGF-A in vehicle/IL-6 treated co-culture, plus 24h treated NPC and MGL
257 monoculture media (N = 3 healthy male donors M3_CTR, 014_CTM and 127_CTM)
258 was measured using a custom U-Plex Biomarker Group 1 (Human) Multiplex Assay
259 (K15067M-1, Meso Scale Discovery), following the manufacturer's instructions.
260 Antibodies for each of the four analytes were cross-linked to a unique spot in each well
261 of a 96-well plate. Each sample was incubated for 2 hours on the plate in technical
262 triplicate, in addition to a seven-point standard curve. A secondary detection antibody
263 was then added and incubated for 2 hours. The plate was read on an MESO QuickPlex
264 SQ 120MM Imager, and data was obtained using Discovery Workbench 4.0 (Meso
265 Scale Discovery).

266

267 ***RNA extraction, RNA Library Preparation and NovaSeq Sequencing***

268 **RNA extraction:** In total, N=4 donors were differentiated for co-culture IL-6 treatment,
269 providing a total of 8 samples for downstream bulk RNA sequencing (RNAseq)
270 analysis. Cells cultured for RNA extraction were collected at RT in TRI Reagent™

271 Solution (Invitrogen; AM9738) by splashing the cells with TRI Reagent™ Solution
272 using a p1000, after removing media and stored at -80ºC. 1ml of TRI Reagent™
273 Solution per 6-well was used for NPCs, and 0.5ml of TRI Reagent™ Solution per 6-
274 well was used for MGLs. RNA was extracted from each sample by centrifugation with
275 200µl of 100% Chloroform (10,000 x *g* for 5 minutes at 4ºC). The top aqueous layer
276 was moved to a new 1.5ml tube with 500µl of 100% isopropanol and mixed 10 times
277 by inversion and incubated 15 minutes at RT. Then, RNA was precipitated by
278 centrifugation (17,000 x *g*, 15 minutes at 4ºC). The supernatant was removed, and the
279 pellet was washed in 1ml of 80% ethanol followed by centrifugation (20,000 x *g*, 5
280 minutes at 4ºC). The ethanol was then removed, the pellet air dried for 15 minutes at
281 RT and then dissolved in 30µl of nuclease free water. Precipitation of RNA by 0.3M
282 Sodium-acetate and 100% ethanol at -80ºC overnight was done to clean samples
283 further, before an additional 80% ethanol wash and subsequent resuspension in 30µl
284 RNAse-free water. Nucleic acid content was measured using NanoDrop™ One.

285

286 **Library Preparation and NovaSeq Sequencing:** Total RNA was submitted for
287 sequencing at Genewiz Inc (South Plainfield, NJ). The following library reparations
288 and RNA sequencing was carried out by Genewiz. Libraries were prepared using a
289 polyA selection method using the NEBNext Ultra II RNA Library Prep Kit for Illumina
290 following manufacturer's instructions (NEB, Ipswich, MA, USA) and quantified using
291 Qubit 4.0 Fluorometer (Life Technologies, Carlsbad, CA, USA). RNA integrity was
292 checked with RNA Kit on Agilent 5300 Fragment Analyzer (Agilent Technologies, Palo
293 Alto, CA, USA). The sequencing libraries were multiplexed and loaded on the flowcell
294 on the Illumina NovaSeq 6000 instrument according to manufacturer's instructions.
295 The samples were sequenced using a 2x150 Pair-End configuration v1.5. Image

296 analysis and base calling were conducted by the NovaSeq Control Software v1.7 on
297 the NovaSeq instrument.

298

299 Upon receipt of FASTQ files from Genewiz, the subsequent bioinformatic analysis
300 were performed. Files were quality controlled using Fastqc (Wingett and Andrews,
301 2018) and aligned to the human reference genome (GRCh38) with STAR (Dobin *et*
302 *al.*, 2013), then sorted and duplicates removed with samtools version 1.13 (Li *et al.*,
303 2009) and Picard version 2.26.2 respectively, all within the King's CREATE high
304 performance computing systems (King's College London, 2022). Downstream gene
305 expression analyses were carried out in R version 4.0.2 (R Core Team, 2020). A count
306 table was prepared and filtered for counts ≥ 1 using featureCounts (Liao *et al.*, 2014)
307 from the Rsubread (Liao, Smyth and Shi, 2019) package, version 2.4.3. Differential
308 gene expression analysis was carried out using DESeq2 (Love, Huber and Anders,
309 2014) version 1.30.1 and the default Wald test. Subsequently, using the Benjamini-
310 Hochberg (BH) method for p-value correction, only genes that passed 5% FDR were
311 considered differentially expressed and submitted for downstream analyses.

312

313 ***Over-Representation and MGEnrichment Analyses***

314 Over representation analysis (ORA) was carried out using WebGestalt (Liao *et al.*,
315 2019), where differentially expressed genes were tested for over representation of
316 non-redundant cellular component, biological process and molecular function gene
317 ontology terms. This analysis used as a background list all genes considered
318 expressed in our model, according to DESeq2s's internal filtering criteria (i.e., adjusted
319 p ≠ NA). Enrichment p-values were corrected for multiple testing using the BH method,

320 and only terms that passed 5% FDR were considered significant. To understand the
321 similarity of the microglial gene sets generated to those from other publications, the
322 MGEnrichment tool was used (Jao and Ciernia, 2021). Genes that were either up- or
323 down- regulated (passing 5% FDR) were imputed into the tool, backgrounded as
324 above. Only human pathways that were enriched were selected, and modules were
325 considered significant if they passed 5% FDR after BH multiple testing correction.

326

327 ***Immunocytochemistry***

328 Cells were fixed with 4% paraformaldehyde (w/v; made in 4% sucrose PBS) for 20 min
329 at room temperature. Samples were then washed twice in PBS, then simultaneously
330 permeabilized and blocked with 2% normalised goat serum (NGS) PBS + 0.1 % Triton
331 X-100 for 2 hours at RT. All antibodies (Supplementary Table 2) were diluted in 2%
332 NGS in PBS. Primary antibodies were incubated with cells overnight at 4ºC, and
333 secondary antibodies were incubated with cells for 1 hour at RT, both in humidified
334 chambers. Between incubations, cells were washed three times in PBS at 15 min
335 intervals. Finally, cells were incubated for 10 min in PBS + DAPI (1:50,000). After the
336 final DAPI stain, cells were left in 150µl/well PBS ready for imaging on an OperaPhenix
337 high throughput imaging system (Perkin Elmer) using a 20x water objective over 6 to
338 10 consistent fields of view per well. Overall, there were 3 to 4 technical repeat wells
339 per staining condition on each plate, coupled with 2 primary-negative wells and 2
340 secondary-negative wells.

341

342 **pSTAT3/tSTAT3 Assay:** Dual SMADi hiPSC-derived NPCs at D21 from three donor
343 lines (127_CTM, 014_CTM and M3_CTR) were thawed and seeded at 25k cells per

344 well directly into a 96-well plate for imaging. After 48h, they were treated for 24h, 3h,
345 30mins and 15mins with Vehicle (Acetic acid), IL-6 100ng/ml, Vehicle + rIL6Ra
346 100ng/ml or IL-6 + rIL6Ra. Cells were stained for TUBB3, STAT3 and phospho-
347 (p)STAT3 and imaged as previously mentioned (Supplementary Table 2). Harmony
348 software (Perkin Elemer) was used to identify nuclei, and the cytoplasm of each cell
349 based on the TUBB3 stain. The raw intensity for pSTAT3 and total STAT3 was
350 measured in both the nuclear and cytoplasmic compartments for each cell.

351

352 **Cell-Marker Expression Assay:** On day 50 of neural differentiation, 29 days after
353 seeding at a density of 30,000 cells/well into 96-well Perkin Elmer CellCarrier Ultra
354 plates, cells were fixed and stained. Cortical neurons were ICC stained with DAPI and
355 TUBB3 to identify morphological boundaries, alongside glial fibrillary acidic protein
356 (GFAP) and paired box protein (Pax6) to identify astrocytes and undifferentiated
357 cortical NPCs respectively (Supplementary Table 2). Using the DAPI stain for PAX6
358 given it's expected expression in the nucleus, and TUBB3 stain for GFAP given it's
359 expected expression in the cytoplasm, the number of cells positive for each marker
360 per well was defined by the intensity of marker being above the background, which
361 was calculated from the lowest intensity limit of each channel's background
362 florescence (mean 5 random locations from the primary negative wells). The number
363 of PAX6+, MAP2+ and TUBB3+ cells per well were collated, and relative populations
364 within each donor were calculated as a percentage of total cells counted.

365

366 **Synapse Counting Assay:** Day 50 post-mitotic cortical neurons were fixed and
367 stained in 96-well Perkin Elmer CellCarrier Ultra plates. To identify nuclei and neurite

368 sections on which synapses lie in cortical neurons, DAPI and MAP2 staining was
369 performed respectively (Nieland *et al.*, 2014). In addition, a combination of specific
370 pre- and post-synaptic proteins was utilized for staining, including the pre-synaptic
371 protein, vesicular glutamate transporter 1 (vGlut1) and post-synaptic protein,
372 postsynaptic density protein 95 (PSD95), or Synaptic vesicle glycoprotein 2A (SV2A,
373 pre-synaptic) and the N-methyl-D-aspartate receptor subunit GluN1(post-synaptic)
374 (Supplementary Table 2). Furthermore, the staining also involved a combination of
375 inhibitory synaptic proteins, Gephyrin (post-synaptic) and glutamate decarboxylase
376 (GAD67; pre-synaptic) (Supplementary Table 2) (Shum *et al.*, 2015, 2020; Deans *et*
377 *al.*, 2017). The following assay analysis was carried out using an automatic script,
378 applied to all replicate wells across donor plates using the Harmony software (Perkin
379 Elemer), with an average of 1400 cells/donor. Initially, MAP2+ cells were identified
380 (Supplementary Figure 5). Then, dendrites were automatically identified using the
381 MAP2+ cell masks, using a Harmony software-integrated algorithm
382 (http://www.csiro.au) (Supplementary Figure 5). Along each dendrite, pre- and post-
383 synaptic puncta were then identified separately from either the 568nm or 488nm
384 imaging channel depending on the secondary antibodies used. Synaptic puncta were
385 thresholded by two characteristics: size and intensity. Synaptic puncta sizes were
386 considered to be between 27-170 pixels, which equated to between 0.8-5μm^2 (Glynn
387 and McAllister, 2006). To calculate the lowest intensity limit, the intensity of each
388 channel's background fluorescence was taken and averaged from 5 random locations
389 from the primary negative wells. To identify maximum intensity, fluorescence intensity
390 from 5 clear artefacts in the primary negative wells were averaged. The dendrite length
391 of MAP2+ cells was measured and averaged per well, to normalise the number of
392 puncta for culture and dendrite outgrowth. This gave two outputs for each puncta

393 channel: intensity and puncta number/dendrite length (density) (Supplementary Figure
394 5). Finally, positively identified puncta were masked on top of each other, to count
395 those that co-colocalised (50% positively overlapped). For each donor, synaptic
396 puncta metrics were averaged from all replicate images for each condition. To reduce
397 the possibility of confounding results caused by staining differences across donor
398 replicate plates, all IL-6 treated puncta metrics were normalised to the vehicle average
399 to create a fold change value from vehicle within donor.

400

401 ***Statistical Analysis***

402 All statistical analyses were conducted using Prism 9 for macOS version 9.3.1
403 (GraphPad Software LLC, California, USA), except for the RNAseq analyses which
404 were carried out using the research computing facility at King's College London,
405 CREATE, along with R version 4.0.2 (R Core Team, 2020). Each specific test
406 performed is described in the corresponding figure legend and supplementary
407 statistical data table, providing the number of replicate hiPSC lines included in each
408 technical and biological replicate, as specified in the relevant method section above.
409 In general, when discussing co-culture data, the N=4 donors (Supplementary Table 1)
410 were considered biological replicates, and when discussing mono-culture data the
411 N=3 donors (3 ♂ only, Supplementary Table 1) were considered biological replicates.
412 To compare post-mitotic cell marker populations, two-way ANOVA was used with cell
413 type and treatment condition as main factors. When assessing the effect of IL-6 on
414 each synaptic metric measured in post-mitotic neurons, one-sample Welch's t-test was
415 used due to the unequal variances between each group in the fold-change values from
416 the vehicle-treated condition (all vehicle donor points = 1). To compare the
417 concentrations of cytokines and sIL-6Ra in control and IL-6 treated co-culture media,

418 an unpaired two-tailed t-test was employed. When comparing the mean between two
419 distinct conditions, such as the concentrations of cytokines in control and IL-6 treated
420 monoculture media from NPCs and MGLs, a two-way ANOVA was employed. For
421 each of the cases in which a t-test was used to compare two group means, an unpaired
422 form of t-test was used, given each cell culture sample is unique and does not reflect
423 a paired design. In the cases where significant differences were observed between
424 groups in these models, post-hoc testing was conducted using the Benjamini-
425 Hochberg (BH) method with a false discovery rate (FDR) of 5% to identify the individual
426 groups with significant differences. Adjusted p-values (q-values) less than 0.05 were
427 considered statistically significant, and relevant significant q-values are quoted. The
428 BH correction method with a 5% FDR threshold was also employed when deciphering
429 the differentially expressed genes from each transcriptome signature, and during the
430 RNAseq downstream over representation analysis.

431 **Results**

432 ***Forebrain neural progenitor cells only respond to IL-6 by trans-signalling in the***
433 ***presence of sIL-6Ra in a dose-dependent manner***

434 To investigate whether forebrain NPCs can respond to IL-6 via trans-signalling using
435 sIL-6Ra, we introduced recombinant human sIL-6Ra (rIL-6Ra) to forebrain NPC
436 monocultures derived from three male donors without a psychiatric diagnosis (one
437 clone each) at day (D) 18 of differentiation. We measured the phosphorylation of
438 STAT3 protein (pSTAT3) levels via immunoblotting to determine if exogenous rIL-6Ra
439 could facilitate a response to IL-6 (Figure 1A, Supplementary Figure 6). Following the
440 combined treatment of 100ng/ml rIL-6Ra and 100ng/ml IL-6, we observed a significant
441 increase in STAT3 phosphorylation in D18 NPCs after 15 minutes (one-way ANOVA

442 F(3, 8) = 1773, $p < 0.0001$), which, while reduced, remained detectable at 3 hours
443 (one-way ANOVA F(3, 8) = 4.920, p = 0.0318) (Figure 1B). Although SHP2
444 phosphorylation by JAK, which induces the Ras-ERK pathway downstream of IL-6
445 signaling, has been previously described in mouse immortalized fibroblasts
446 (Fiebelkow *et al.*, 2021), phosphorylation of ERK1/2 was not detected in NPCs after
447 15min (one-way ANOVA: F (3, 8) = 0.8869, p = 0.4881) or 3h (one-way ANOVA: F (3,
448 8) = 2.458, p = 0.1375) of IL-6 exposure, with or without rIL-6Ra (Supplementary
449 Figure 7). Regarding STAT3 phosphorylation, a dose-dependent relationship was
450 evident when varying rIL-6Ra concentrations (Figure 1C, Supplementary Figure 6).
451 Lower doses corresponded to reduced pSTAT3/tSTAT3 ratios after 15 minutes of IL-
452 6 exposure (two-way ANOVA: Interaction F(4, 20) = 31.94, $p < 0.0001$; [rIL-6Ra]
453 Factor F(4, 20) = 36.55, $p < 0.0001$; Treatment Factor F(1, 20) = 436.0, $p < 0.001$)
454 (Figure 1D, statistics in Supplementary Table 3). Notably, at the lowest dose (1ng/ml
455 rIL-6Ra), there was no statistical difference between pSTAT3/tSTAT3 levels in vehicle
456 and IL-6 treated NPCs (5% FDR = 0.371).

457

458 To determine if a subpopulation of hiPSC-derived NPCs could respond to IL-6 without
459 the presence of rIL-6Ra after 15min, 30min, 3h or 24h of stimulation,
460 immunocytochemistry was used to stain for pSTAT3 and total STAT3 (Figure 1E, full
461 timepoint images in Supplementary Figure 8). pSTAT3 intensity increased in both the
462 nuclear and cytoplasmic compartments of NPCs exposed to a combined treatment of
463 100 ng/ml rIL-6Ra and 100 ng/ml IL-6 (Figure 1F), peaking after 30 minutes of
464 exposure (Two-way ANOVA Cytoplasmic pSTAT3: treatment p = 0.002, timepoint =
465 0.382, interaction p = 0.173. Nuclear pSTAT3 intensity: treatment $p = 3.84 \times 10^{-11}$,
466 timepoint p = 0.245, interaction p = 0.016). Although the intensity of total STAT3

467 remained unaffected by treatment in both compartments at all timepoints measured,
468 there was an increased total STAT3 signal in all treatment groups after 24h of
469 exposure (Two-way ANOVA Cytoplasmic STAT3: treatment $p = 0.667$, timepoint =
470 0.203, interaction $p = 0.913$. Nuclear STAT3 intensity: treatment $p = 0.276$, timepoint
471 $p = 0.019$, interaction $p = 0.533$). When comparing the total population of cells
472 measured in density plots, no distinct subpopulation of NPCs responded to 100 ng/ml
473 IL-6 without rIL-6Ra, as increased pSTAT3 signal intensity shifts were only observed
474 in cells treated with both 100 ng/ml IL-6 and 100 ng/ml rIL-6Ra (Figure 1G, cell
475 numbers per condition in Supplementary Table 4).

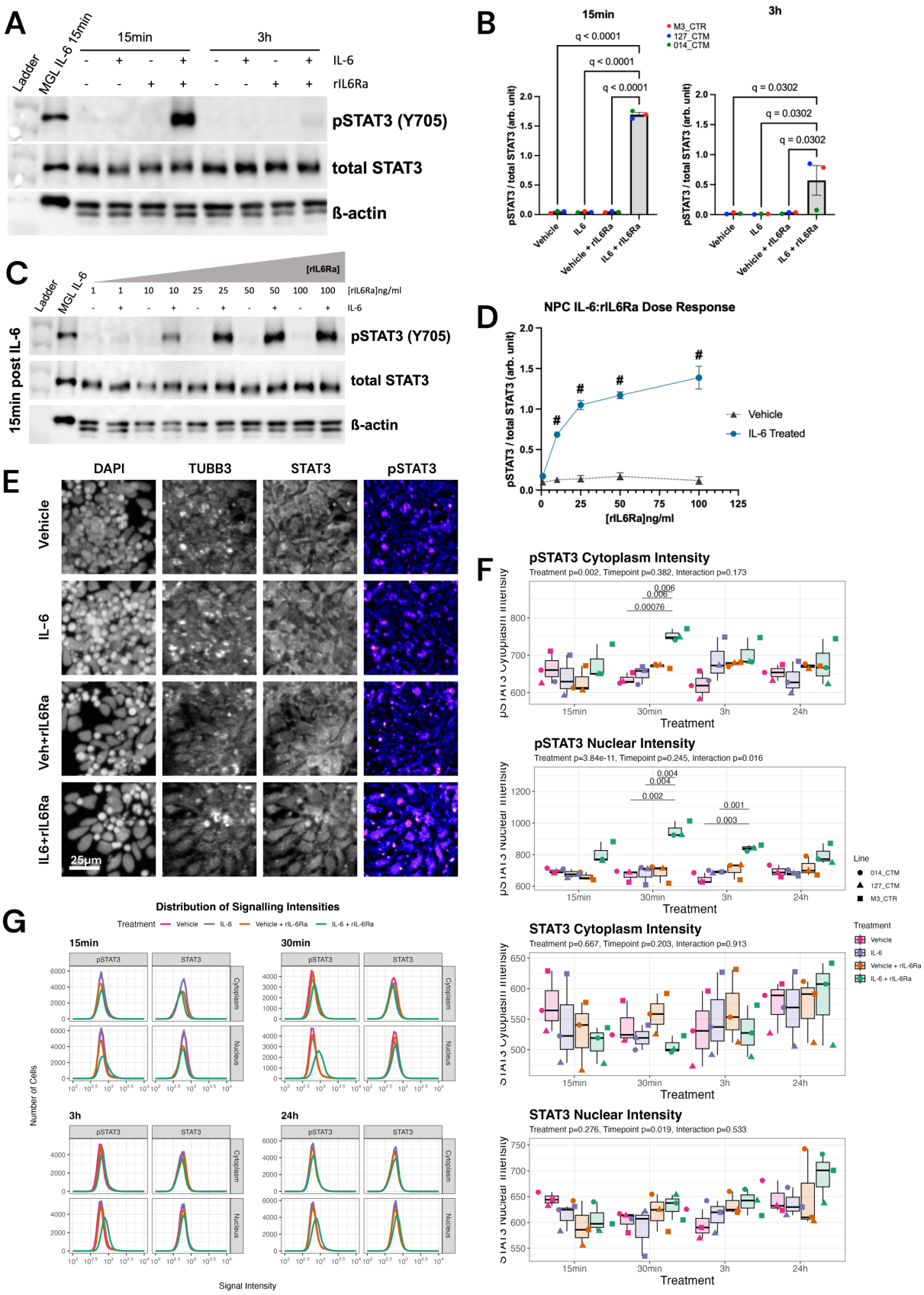

Figure 1 – Demonstrating Trans-Signalling Capability of Cortical Neural Progenitor Cells with IL-6 in Monoculture. (A) Immunoblot depicting pSTAT3 (88kDa), tSTAT3 and β-Actin protein levels in D18 NPC monocultures. Samples, treated with vehicle or 100ng/ml IL-6 coupled with or without 100ng/ml of sIL-6Ra, were

480 collected at 15 minutes and 3 hours for comparison. Full length, uncropped images can be found in Supplementary
481 Figure 6. (B) Quantitative assessment of pSTAT3/tSTAT3 protein ratios from blot (A) at 15 minutes and 3 hours
482 post-stimulation. Measurements are in arbitrary units, presented as mean ± standard deviation (SD). Statistical
483 significance determined by one-way ANOVA with 5% FDR (Benjamini–Hochberg method) is indicated. Data
484 derived from N=3 neurotypical male hiPSC cell lines, each with one technical replicate. Data points are colour-
485 coded per donor line: red for M3_CTR, blue for 127_CTM, and green for 014_CTM. (C) Immunoblotting results
486 showing 88kDa pSTAT3/tSTAT3 and β-Actin in response to a gradient of rIL-6Ra concentrations (1, 10, 25, 50,
487 and 100 ng/ml) combined with 100ng/ml IL-6. Samples collected after 15 minutes of stimulation in D18 NPC
488 monocultures. Full length, uncropped images can be found in Supplementary Figure 6. (D) Line graph quantification
489 of pSTAT3/tSTAT3 protein ratios from blot (C) at 15 minutes and 3 hours, presented in arbitrary units. Data points
490 are mean ± SD, with colour-coding indicating treatment conditions as per the key. Two-way ANOVA results, with
491 adjustments for multiple comparisons and a q-value < 0.0001 after 5% FDR correction, are marked with '#' for IL-
492 6 treatment vs. vehicle comparisons. Data based on N=3 neurotypical male hiPSC cell lines, each with one
493 technical replicate. (E) Representative images of hiPSC-derived NPCs at D24 from donor line 127_CTM, treated
494 for 30mins with vehicle, IL-6 100ng/ml, vehicle + rIL6Ra 100ng/ml or IL-6 + rIL6Ra. Cells were stained for TUBB3,
495 STAT3 and phospho-STAT3. These representative images are 4x digitally zoomed from the full original 20x images
496 available in Supplementary Figure 8. White scale bar represents 25μm. (F) Boxplots of raw staining intensities for
497 pSTAT3 and total STAT3 in both the nuclear and cytoplasmic compartments of D24 hiPSC-derived NPCs. Each
498 point represents the donor mean value from three technical replicate wells per condition, imaged 6 times per well.
499 Comparison of treatment and timepoint variables were made using a two-way ANOVA, with the p-values printed
500 above boxplots. Significant post-hoc comparisons for each sample are labelled above relevant comparison. (G)
501 Distribution plots of signalling intensities across all cells measured across three donor lines (M3_CTR, 127_CTM
502 and 014_CTM). Distributions are split into pSTAT3 and STAT3 stains, in both the cytoplasm and nucleus
503 compartments of the cells. Each treatment condition is defined by a different coloured line.

504

505 ***The concentration of sIL6Ra released from hiPSC-derived MGLs may not be***
506 ***sufficient to induce trans-signalling in NPCs***

507 If NPCs in co-culture are to respond via trans-signalling to IL-6, then the presence of
508 sIL-6Ra secreted by microglia is required. To confirm this, we measured sIL-6Ra
509 concentrations in an MGL-NPC co-culture media using ELISA (Figure 2A). The results
510 confirm the presence of the soluble receptor, but there were no significant changes in
511 sIL-6Ra concentration after 24h of IL-6 exposure (unpaired two-tailed t-test t(6) =
512 0.180, R2 = 0.005, p = 0.863). The average sIL-6Ra concentration in the co-culture
513 media was 0.29 ± 0.03 ng/ml (range: 0.27 to 0.31 ng/ml), which is lower than the
514 average sIL-6Ra concentration typically found in human cerebrospinal fluid (CSF):

515 approximately 1.3 ± 0.6 ng/ml in inflammatory patients (meningitis symptoms with
516 pleocytosis) and 0.9 ± 0.5 ng/ml in non-inflammatory patients (meningitis symptoms
517 without pleocytosis) (Azuma *et al.*, 2000). Of note, the Asp358Ala A>C *IL6R* variant is
518 known to increase sIL-6Ra secretion whilst conversely reduce a cell's overall
519 responsiveness to IL-6 (Ferreira et al., 2013; Khandaker et al., 2014). Therefore, we
520 next characterized this SNP in our donor lines to mitigate potential confounding effects
521 on our ELISA results. Genotyping revealed that all donor lines used in this study
522 possessed the C/C allele (Supplementary Table 5). To understand the secretion
523 dynamics of sIL-6Ra from MGLs over time, we measured the concentration of sIL-6Ra
524 in the media after 0, 3, 6, 12, 24, and 48 hours of exposure to either vehicle or 100
525 ng/ml IL-6 in monoculture (N=3 independent differentiations; Figure 2B). The data
526 confirmed an accumulation of sIL-6Ra in the media over time, with no significant effect
527 of treatment (two-way ANOVA: treatment $F(1,24) = 1.596$, $p = 0.219$; time $F(5,24) =$
528 4.804, $p = 0.0035$; interaction $F(5,24) = 0.797$; $p = 0.563$). Overall, our findings indicate
529 that although the sIL-6Ra receptor is present, the co-culture system concentration
530 might still be insufficient for effective NPC trans-signalling during the 24-hour exposure
531 period in the experimental set-up chosen.

532

533 Irrespective of IL-6 trans-signalling in the NPCs, we hypothesized that NPCs might
534 additionally react to other cytokines produced by MGLs in response to IL-6 stimulation.
535 To investigate this, we used a qualitative cytokine profiler to characterize the cytokine
536 and chemokine milieu in the co-culture media following 24 hours of exposure to IL-6
537 or a vehicle control (Figure 2C). This analysis included a panel of 105 cytokines and
538 chemokines (Supplementary Figure 4, Supplementary Table 6). We observed that
539 osteopontin, IL-8, ENA-78, and MMP-9 were the most abundant molecules in the co-

540 culture media across both treatment groups (Figure 5D). Relative to the vehicle control,
541 IL-6 exposure led to increased signals in 78 molecules and a decrease in 26. The five
542 most upregulated molecules were MIP-1α/MIP-1β (Fold Change (FC) = 4.153),
543 RANTES (FC = 2.118), GROα (FC = 2.105), TNF-α (FC = 1.689), and PF4 (FC =
544 1.593). Conversely, the most significantly downregulated molecules included anti-
545 inflammatory ligands Lipocalin-2 (FC = 0.69), PDGF-AA (FC = 0.69), LIF (FC = 0.82),
546 and Fas Ligand (FC = 0.88).

547

548 To corroborate the findings from the proteome profiler assay, we quantitatively
549 measured four cytokines using a multiplex cytokine assay by Meso Scale Diagnostics
550 (Figure 2E). MIP-1α and TNF-α were selected for their upregulation in response to IL-
551 6, while IL-8 served as a negative control due to its consistent secretion levels in both
552 vehicle and IL-6 treated media. Additionally, VEGF was included due to its role in
553 angiogenesis and neurodevelopment, given its observed increased expression in
554 chronic medicated SZ patients (Chukaew *et al.*, 2022) and in foetal mouse brains from
555 an MIA rodent model (Poly I:C on gestational day 16) (Arrode-Brusés and Brusés,
556 2012). Consistent with our expectations, IL-8 levels remained stable with IL-6
557 treatment (unpaired two-tailed t-test: Fold Change (FC) = 1.22, $t(6) = 1.603$, $R^2 = 0.30$,
558 $p = 0.160$). MIP-1α and TNF-α showed an increase following IL-6 treatment, though
559 not reaching statistical significance (MIP-1α unpaired two-tailed t-test: Fold Change
560 (FC) = 2.48, $t(6) = 1.531$, $R^2 = 0.281$, $p = 0.177$; TNF-α unpaired two-tailed t-test: FC
561 = 13.75, $t(6) = 1.180$, $R^2 = 0.188$, $p = 0.283$). In contrast, VEGF-A levels did not
562 significantly change with IL-6 treatment (unpaired two-tailed t-test: FC = 1.155, $t(6) =$
563 0.156, $R^2 = 0.004$, $p = 0.884$). Overall, the expression patterns of these cytokines
564 quantitatively measured by the multiplex cytokine assay aligned with the qualitative

565 trends observed in the proteome profiler assay, reinforcing our understanding of the
566 cytokine response to IL-6 in our experimental setup.

567

568 Finally, to elucidate the source of cytokine secretion in our co-culture system, we
569 examined the same cytokine candidates in 24-hour IL-6 treated D14 MGL and D18
570 NPC monocultures derived from N = 3 neurotypical male cultures (Figure 2F, with two-
571 way ANOVA statistics provided in Supplementary Table 7). Our analysis indicated that
572 MGLs were predominantly responsible for secreting IL-8, MIP-1α, and TNF-α,
573 whereas VEGF secretion was mainly attributed to NPCs. Notably, TNF-α was the only
574 cytokine to demonstrate a statistically significant increase in response to IL-6
575 treatment in MGLs (MGL Vehicle vs MGL IL-6, q = 0.015), but not in NPCs. Together,
576 the data provide insights into the cytokine milieu downstream of IL-6 signalling in an
577 MGL-NPC co-culture system, and the cytokines to which NPCs may respond within
578 the co-culture environment in addition to direct IL-6 trans-signalling.

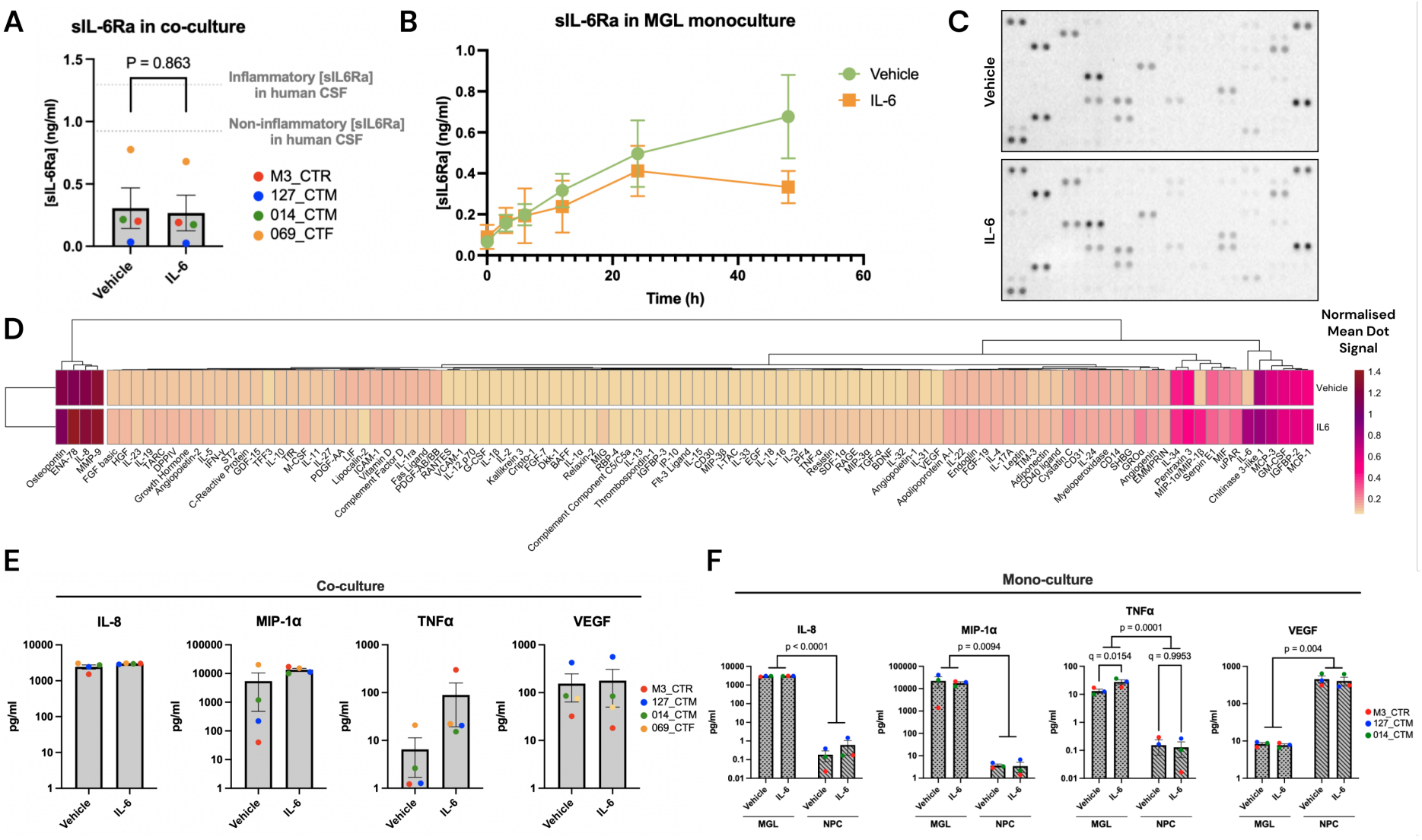
A
sIL-6Ra in co-culture
P = 0.863
Inflammatory [sIL6Ra] in human CSF
Non-inflammatory [sIL6Ra] in human CSF
[sIL-6Ra] (ng/ml)
M3_CTR
127_CTM
014_CTM
069_CTF
Vehicle
IL-6
B
sIL-6Ra in MGL monoculture
[sIL6Ra] (ng/ml)
Time (h)
Vehicle
IL-6
C
Vehicle
IL-6
D
Normalised Mean Dot Signal
Vehicle
IL6
E
Co-culture
IL-8
MIP-1α
TNFα
VEGF
pg/ml
M3_CTR
127_CTM
014_CTM
069_CTF
F
Mono-culture
IL-8
p < 0.0001
MIP-1α
p = 0.0094
TNFα
p = 0.0001
q = 0.0154
q = 0.9953
VEGF
p = 0.004
MGL
NPC

579

580 **Figure 2 - Investigating Indirect Effects of IL-6 Through the MGL Cytokine Secretion Response.** (A) The sIL-
581 6Ra concentration in co-culture media (ng/ml) varied by donor without significant IL-6 treatment effects. Data points
582 are color-coded by donor and presented as mean ± SD. Reference lines indicate typical human CSF sIL-6Ra levels
583 in control (non-inflammatory) and meningitis (inflammatory) cases, based on Azuma et al. (2000). (B) The sIL-6Ra
584 concentration (ng/ml) in hiPSC-derived MGL monoculture media (N=3 myeloid factory differentiations of the
585 KOLF2.1J line) accumulates through time to 48h but does not reach the concentration found in human CSF. (C)
586 The cytokine profiles in vehicle and IL-6 treated NPC-MGL co-cultures as measured by dot blot images comparing
587 cytokine secretion, using the Proteome Profiler Human XL Cytokine Array Kit (R&D Systems) measuring 104
588 cytokines (N = 4 donors pooled per condition). Cytokine and chemokine labels provided in supplementary material.
589 (D) Heatmap of average raw cytokine signal, corrected for background and normalised to positive reference values
590 per membrane, from the Proteome Profiler Array. Plotted are averaged raw signal values from 2 technical replicates
591 per cytokine, with IL-6 added during treatment. (E) Concentrations of MIP-1a, TNF-α, IL-8, and VEGF-A measured
592 in co-culture media after 24h with vehicle or 100ng/ml IL-6 treatment (N = 4, grey bars), as measured by the MSD
593 multiplex cytokine assay. Data plotted as pg/ml on a log scale. Bar graphs show mean ± SD, with each point
594 representing one donor line, and coloured as such. (F) Concentrations of MIP-1a, TNF-α, IL-8, and VEGF-A in
595 monoculture media from control donors (N = 3 males) D14 MGLs and D18 NPCs, treated for 24h with vehicle or
596 100ng/ml IL-6, as measured by the MSD multiplex cytokine assay. Data plotted as pg/ml on a log scale. 5% FDR
597 corrections post two-way ANOVA indicated. Bar graphs represent mean ± SD, color-coded by donor line.

598

599 ***The impact of acute IL-6 on hiPSC-derived MGL transcriptome after 24h***

600 We next conducted bulk RNAseq analysis to characterize and confirm the overall
601 transcriptional response of hiPSC-derived microglia-like cells (MGLs) in co-culture
602 with neural progenitor cells (NPCs) to IL-6. Principal component analysis (PCA) of
603 each sample highlighted the most significant variance in the MGL transcriptome: donor
604 genetic background (PC1 = 58% variance explained) and IL-6 treatment (PC2 = 19.64%
605 variance explained) (Figure 3A). Notably, the only female donor (069_CTF) exhibited
606 distinct separation on the PC1 axis from male donors, but due to inclusion of a single
607 female hiPSC line, further sex-based analysis was not pursued. Subsequent analysis
608 revealed 72 differentially expressed genes (DEGs) post-IL-6 exposure (out of 16820
609 genes measured) after FDR correction at 5%. As anticipated, similarly to our prior
610 study with IL-6 stimulated MGL mono-cultures (Couch *et al.*, 2023), IL-6 receptor
611 signal transduction genes like *JAK3* and *STAT3* were significantly upregulated (Figure

612 3B). The most upregulated gene was *EBI3*, known for mediating IL-6 trans-signalling,
613 albeit less efficiently than sIL-6Ra (Chehboun *et al.*, 2017). These results confirm
614 successful IL-6 stimulation in control MGLs in co-culture.

615

616 We also validated the MGL differentiation from hiPSCs and assessed if IL-6
617 stimulation influenced their inherent cell type identity. The DESeq2 normalized counts
618 of human microglia and monocyte marker genes were compared between vehicle-
619 treated and IL-6 treated samples (Figure 3C). This comparison was based on a gene
620 list from Haenseler et al. (2017), including genes highly expressed in human microglia
621 (Melief *et al.*, 2012) and *TMEM119*, a microglia-specific gene (Bennett *et al.*, 2016).
622 Our findings align with the expression profile of microglial marker genes as per the
623 original MGL differentiation protocol, and no significant clustering was observed based
624 on IL-6 treatment, suggesting that IL-6 exposure did not alter MGL cell-specificity at
625 the gene expression level, consistent with previous data (Couch *et al.*, 2023).

626

627 To explore the molecular pathways influenced by IL-6 receptor signalling in MGLs in
628 co-culture with NPCs, we conducted a Webgestalt over-representation analysis (ORA)
629 on the up- and down-regulated gene sets (Liao *et al.*, 2019) (Figure 3D). The down-
630 regulated gene set showed no significant associations with ORA pathways post-FDR
631 correction ($q > 0.05$). In contrast, 24 pathways were significantly linked with
632 upregulated genes, including “STAT cascade”, “Interleukin-6 production”, and “acute
633 inflammatory response” (Figure 3D). The pathway “positive regulation of cell motility”
634 was also notably associated, supporting previous findings that IL-6 stimulation
635 enhances microglial motility (Ozaki *et al.*, 2020; Couch *et al.*, 2023). These data

636 suggest that the observed terms related to the IL-6 pathway, along with others
637 pertaining to cellular recruitment and cell-to-cell adhesion (such as "leukocyte
638 migration", "T-cell activation", and "regulation of cell-cell adhesion"), point towards an
639 acute, pro-inflammatory functional shift by the microglia to an acute 24h stimulation
640 with IL-6 in co-culture with NPCs.

641

642 To understand if the IL-6-induced transcriptional changes in MGLs after 24 hours
643 mirror those observed in neurodevelopmental disorders, we performed gene set
644 enrichment analysis (GSEA) (Figure 3E). The analysis overlapped each signature with
645 gene sets from post-mortem brain tissue of individuals with schizophrenia (SZ), autism
646 spectrum conditions (ASC), and bipolar disorder (BD). Notably, the MGL transcriptome
647 post-IL-6 exposure showed significant enrichment for the up-regulated gene set from
648 SZ patients (list of overlap genes in Supplementary Table 8). Webgestalt ORA
649 identified several enriched pathways, including “lymphocyte activation”, “adaptive
650 immune response”, and “T cell activation” (Figure 3F). Collectively, these findings
651 imply that the IL-6 response of MGLs in co-culture mirrors that observed in
652 monocultures (Couch *et al.*, 2023), and that the molecular processes identified in SZ
653 *post-mortem* brain tissue are detectable in our developmental *in vitro* model.

654

655 Finally, we aimed to delineate the differences between the MGL transcriptomic
656 response to IL-6 in co-culture versus mono-culture conditions (Couch et al., 2023). To
657 achieve this, we utilised the MGEnrichment tool output to qualitatively compare
658 specifically human modules that were enriched by up-regulated genes in both the
659 mono-culture and co-culture MGLs following IL-6 stimulation (Figure 3G). The

660 enrichment scores derived from our MGEnrichment analysis demonstrated a robust
661 activation of the 'SCZ & ASD & BD Gene Modules' in both the co-culture and mono-
662 culture environments, indicating a highly potentiated upregulation of genes associated
663 with NDDs. Of note, the transcriptomic profiles between mono-culture and co-culture
664 microglia were contrasted, with a more modest NDD-related enrichment score
665 obtained from the mono-culture microglia in comparison to the co-culture (co-culture
666 FE = 12.36, q = 2.14×10^{-11}; mono-culture FE = 5.07, q = 1.8×10^{-13}). These data suggest
667 that the presence of NPCs in a co-culture can modulate microglial gene regulation
668 across various pathways, particularly those related to NDDs, and may suppress the
669 MGL response to IL-6, consistent with previous findings (Haenseler *et al.*, 2017).

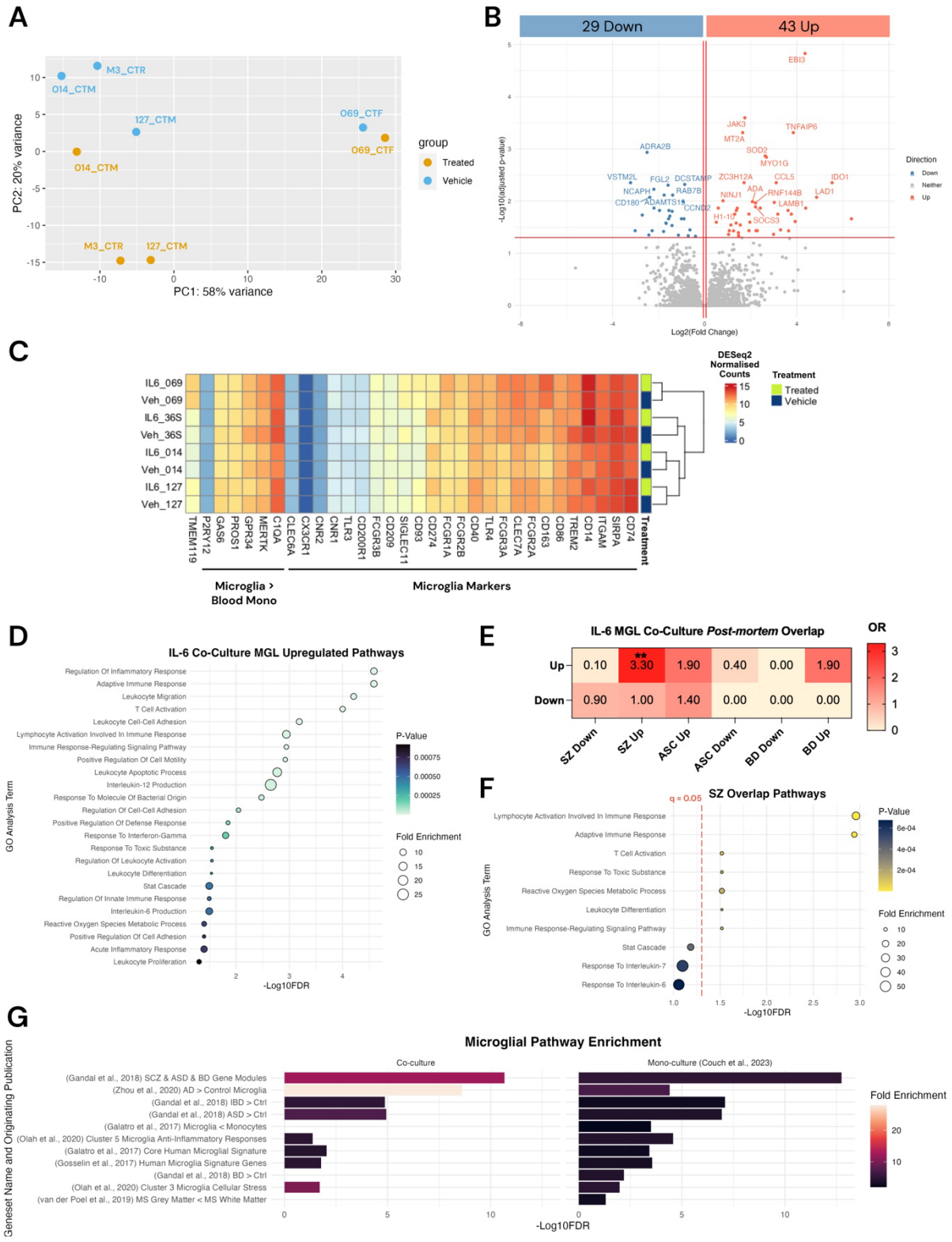

Figure 3 - IL-6 Induces Changes in the MGL Transcriptome in Co-Culture with NPCs. (A) PCA of DESeq2 normalized counts (median of ratios), colour-coded for vehicle (blue) and IL-6 treatment (orange) and identified by donor line. Clustering reveals treatment and donor genotype influences on the MGL transcriptome. (B) Volcano plot highlighting 72 differentially expressed genes in MGLs post 24h IL-6 stimulation in co-culture with NPCs. Genes with log2FoldChange > 0.06 and adjusted p-value < 0.05 are marked in red; those with log2FoldChange < -0.06

676 and adjusted p-value < 0.05 in blue. Top 25 DEGs are labelled. (C) Heatmap of DESeq2 normalized counts (median
677 of ratios) for vehicle-treated MGLs, showing consensus microglial-specific markers, including genes highly
678 expressed in human microglia and those differentially expressed compared to blood monocytes, plus TMEM119.
679 Right-hand side hierarchical clustering indicates no significant treatment-based changes. (D) Webgestalt gene
680 ontology analysis of upregulated genes post-IL-6 treatment in MGLs, with 5% FDR correction. ORA terms sorted
681 by –fadditionalFDR, colour-coded by p-value, and scaled by fold enrichment. (E) Fisher's exact test comparing
682 gene sets from ASC, SZ, and BD post-mortem human tissues (Gandal et al., 2018) with RNAseq-identified up- and
683 down-regulated gene sets. Heatmap of odds ratios (OR) presented, with significance marked as: . q < 0.1, * q <
684 0.05, ** q < 0.01, *** q < 0.001, **** q < 0.0001; non-significant values are unlabelled. (F) Webgestalt gene ontology
685 analysis of the 17 genes common between MGL up-regulated IL-6 and upregulated SZ post-mortem tissue gene
686 sets (Gandal et al., 2018). Analysis is FDR-corrected at 5%, with ORA terms sorted by –log10FDR, colour-coded
687 by p-value, and sized by fold enrichment. Red dotted line signifies q = 0.05, and values to the left of this line do not
688 pass BH FDR correction. (G) MGEnrichment analysis of genes up-regulated in IL-6 stimulated MGLs, in both co-
689 culture and mono-culture settings (Couch et al., 2023), adjusted with a 5% FDR. Enriched gene sets arranged by
690 –log10FDR and colour-coded by fold enrichment.

691

692 ***The proximal impact of IL-6 on hiPSC-derived forebrain NPC transcriptome in***
693 ***co-culture with MGLs***

694 With the knowledge that hiPSC-derived MGLs responded to IL-6 in co-culture with
695 NPCs, we aimed to investigate if NPCs respond to IL-6 via trans-signalling either
696 directly from sIL6Ra secreted by MGLs, or indirectly via other cytokines and
697 chemokines such as TNF-α secreted by MGLs in response to IL-6. Bulk RNAseq was
698 performed on hiPSC-derived NPCs after 24 hours in co-culture with MGLs treated with
699 either IL-6 or vehicle. We first assessed the impact of co-culturing NPCs with MGLs
700 and IL-6 treatment on cell type heterogeneity using the NPC RNAseq dataset (Figure
701 4A). DESeq2 normalized counts were analysed for markers indicative of neural
702 progenitor, pan-neuronal, dorsal forebrain, ventral forebrain, midbrain, hindbrain,
703 upper layer and deep layer cells (Nehme *et al.*, 2018) (Figure 4A). The analysis
704 revealed predominant expression of neural progenitor cell-related genes, consistent
705 with the expected outcome at this differentiation stage. This finding suggests that co-
706 culturing with hiPSC-derived MGLs using trans-well inserts did not alter the anticipated

707 NPC cell type profile, given there was no hierarchical clustering by cell-markers.
708 Clustering was in-fact influenced by donor genotype rather than IL-6 treatment,
709 indicating that the IL-6 exposure did not significantly affect the cell type composition
710 of NPCs at this culture stage.

711

712 Contrary to our hypothesis however, PCA analysis revealed that the most significant
713 variation in the NPC transcriptome was attributable to donor genotype rather than IL-
714 6 treatment (Figure 4B). Out of the 17225 genes measured, only 2 DEGs passed the
715 5% FDR threshold for increased expression in NPCs in co-cultures treated with IL-6
716 versus vehicle, thereby exhibiting a minimal transcriptional difference (Figure 4C):
717 TNF-Alpha-Induced Protein 3 (*TNFAIP3*: q = 0.0282, Log2FC = 1.545) and Poly(A)
718 Binding Protein Cytoplasmic 1 (*PABPC1*: q = 0.0282, Log2FC = 0.1874). The absence
719 of statistically significant changes in JAK/STAT pathway genes (*STAT3* Log2FC =
720 0.0997, p = 0.543, q = 0.9998; *JAK3* Log2FC = 0.584, p = 0.0396, q = 0.9998,
721 Supplementary Figure 9) suggests that the IL-6-receptor signal transduction pathway
722 was not activated in NPCs at the timepoint of analysis, in contrast to MGLs
723 (Supplementary Figure 9). Additionally, the expression of four key downstream genes
724 of the Ras-ERK pathway (*PHLDA1, DUSP4, EPHA2,* and *SPRY4*)(Chesnokov, Yadav
725 and Chefetz, 2022), were found unchanged after IL-6 exposure in both MGLs and
726 NPCs (Supplementary Figure 9). On the other hand, the data suggests that the NPCs
727 might have the potential to react to the TNF-α secreted by MGLs cells, as indicated by
728 the observed upregulation of *TNFAIP3*. In summary, under the conditions tested,

729 forebrain cortical NPCs derived from neurotypical control donors exhibit a negligible

730 transcriptional response to 24-hour IL-6 exposure in co-culture with MGLs.

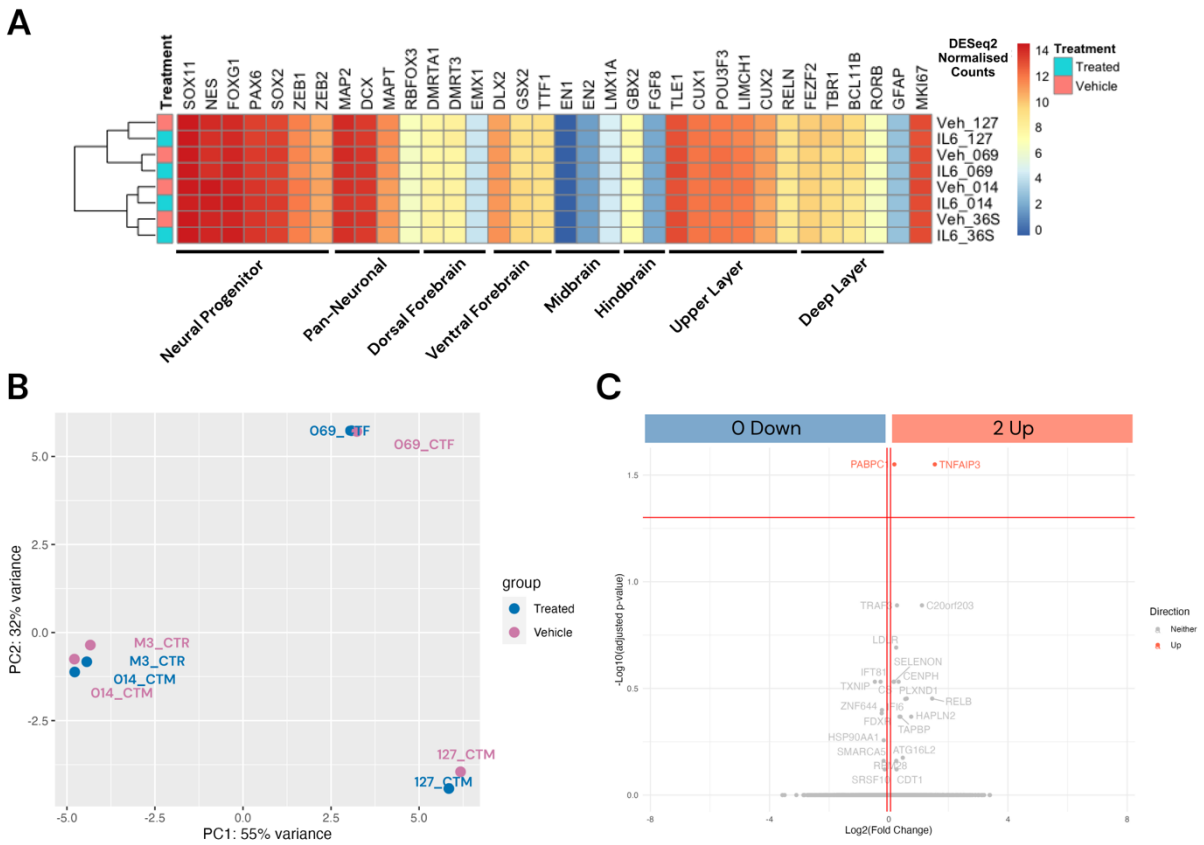

731

732 **Figure 4 - Assessing the Proximal NPC Transcriptome Response to IL-6 in Co-Culture with MGLs.** (A)
733 Heatmap of DESeq2 normalized counts (median of ratios) from vehicle-treated NPCs, displaying cell-specific
734 marker gene expression across both genotypes. (B) PCA plot of DESeq2 normalized data (median of ratios),
735 distinguishing vehicle (pink) and IL-6 treated (blue) samples, with donor line annotations. (C) Volcano plot
736 showcasing NPCs' differentially expressed genes following IL-6 exposure in co-culture with MGLs. Genes with
737 log2FoldChange > 0.06 and adjusted p-value < 0.05 are marked in red; those with log2FoldChange < -0.06 and
738 adjusted p-value < 0.05 in blue. Genes without a significant FDR corrected p-value are coloured grey. The top 25
739 expressed genes are labelled.

740

741 ***The long-term impact of acute NPC-stage IL-6 exposure in terminally***

742 ***differentiated forebrain cortical neurons***

743 To evaluate whether IL-6 exposure to MGL-NPC co-cultures, either directly via trans-

744 signalling or indirectly via the response secretome by MGLs, influenced the

745 differentiation trajectories of forebrain NPCs at D18 in co-culture with MGLs, we
746 analysed the relative proportions of cell types using cell-specific markers (Figure 5A,
747 Supplementary Figure 10). Cell populations expressing TUBB3, GFAP and Pax6 were
748 quantified as a percentage of total cells in terminally differentiated cortical neuron
749 cultures at day 50 of differentiation (Figure 5B, Supplementary Table 9). The results
750 showed that across both treatment groups, 96.66% of all cells were TUBB3+, 17.27%
751 were GFAP+, and 6.38% were Pax6+, consistent with a predominance of neurons in
752 the differentiated cultures. The majority of cells in both treatment groups were
753 TUBB3+/GFAP-/Pax6- (73.43 ± 5.37%), indicating a significant proportion of neurons,
754 followed by cells likely representing foetal astrocytes or radial glia
755 (TUBB3+/GFAP+/Pax6-; 16.72 ± 3.04%) (Dráberová *et al.*, 2008). A limited population
756 only expressed Pax6 (TUBB3-/GFAP-/Pax6+ = 2.82 ± 1.00 %), and with minimal co-
757 expression with TUBB3 (TUBB3+/GFAP-/Pax6+ = 3.49 ± 1.05 %) (Figure 5B). Notably,
758 there were no significant differences in the proportions of cell types between NPCs
759 exposed to IL-6 and those that were not (two-way ANOVA: treatment $F(1,42) =$
760 2.25×10^{-7}, $p = 0.999$; cell-type $F(6,42) = 88.04$, $p < 0.0001$; interaction $F(1=6,42) =$
761 0.38; $p = 0.89$). In summary, these findings indicate that NPCs in co-culture with MGLs
762 differentiated into a range of cell types, predominantly post-mitotic cortical neurons,
763 and that IL-6 exposure did not significantly alter their differentiation towards various
764 cell fates.

765

766 The architecture, number, and source of synaptic connections on neurons critically
767 influence neuronal activity (Kuljis *et al.*, 2019). Furthermore, disruptions in these
768 synaptic properties could be central to the pathogenesis of NDDs (Bayés *et al.*, 2011;
769 Südhof, 2017; Mirabella *et al.*, 2021). We therefore explored whether changes during

770 the NPC stage, either directly by trans-IL-6 signalling or indirectly via cytokines
771 released from IL-6 stimulated MGLs, could induce alterations in synapses. To
772 investigate this, we quantified the density and abundance (by signal intensity) of both
773 inhibitory and excitatory synaptic puncta along MAP2+ neurites, grown until D50 of
774 differentiation. The choice of synaptic markers was informed by their relevance to
775 synaptic transmission and association with neurodevelopmental disorders such as SZ
776 and ASC. Specifically, we focused on PSD95 (Figure 5C), GluN1 (Figure 5D), and
777 vGlut1 (Figure 5C) due to their roles in glutamatergic neurotransmission.
778 Dysregulation in this system has been implicated in the onset of SZ and ASC (Oni-
779 Orisan *et al.*, 2008; Bitanihirwe *et al.*, 2009; Moghaddam and Javitt, 2012; Holloway
780 *et al.*, 2013; De Bartolomeis *et al.*, 2014; Grunwald *et al.*, 2019; Mirabella *et al.*, 2021).
781 Additionally, SV2A (Figure 5D) was included due to its reported decrease in individuals
782 with an SZ diagnosis (Onwordi *et al.*, 2020, 2023). We also assessed GAD67 (Figure
783 5E), known for its consistently decreased expression in the brains of individuals with
784 psychiatric disorders such as SZ, bipolar disorder (BD), and major depressive disorder
785 (MDD) (Miyata et al., 2021; Karolewicz et al., 2010; Hashimoto et al., 2008; Guidotti
786 et al., 2000). Lastly, Gephyrin was examined due to its association with hemizygous
787 microdeletions in the G-domain (Figure 5E), which have been observed in unrelated
788 individuals affected by ASC and SZ (Lionel *et al.*, 2013). However, under the
789 conditions tested, acute 24hr IL-6 exposure at the NPC stage did not significantly
790 affect the densities, nor the abundance of either pre- or post-synaptic protein
791 expression, as measured by the non-parametric Wilcoxon's test (Figure 5G,
792 Supplementary Figure 11). Furthermore, we investigated the co-localization of pre-
793 and post-synaptic proteins: PSD95 with vGlut1, GluN1 with SV2A, and Gephyrin with
794 GAD67 (Figure 5F). The extent of puncta co-localization, interpreted as pre- and post-

795 synaptic connectivity, was quantified and compared between vehicle-treated neurons
796 and those exposed to IL-6. Our results indicate that puncta co-localization was not
797 influenced by early acute IL-6 exposure, as evidenced by the absence of significant
798 differences between the treatment groups (Figure 5H-I). However, there was clearly
799 extensive donor variance in these measures following exposure to IL-6, likely due
800 individual genotype differences. Hence, we cannot conclusively dismiss the possibility
801 of an effect of IL-6.

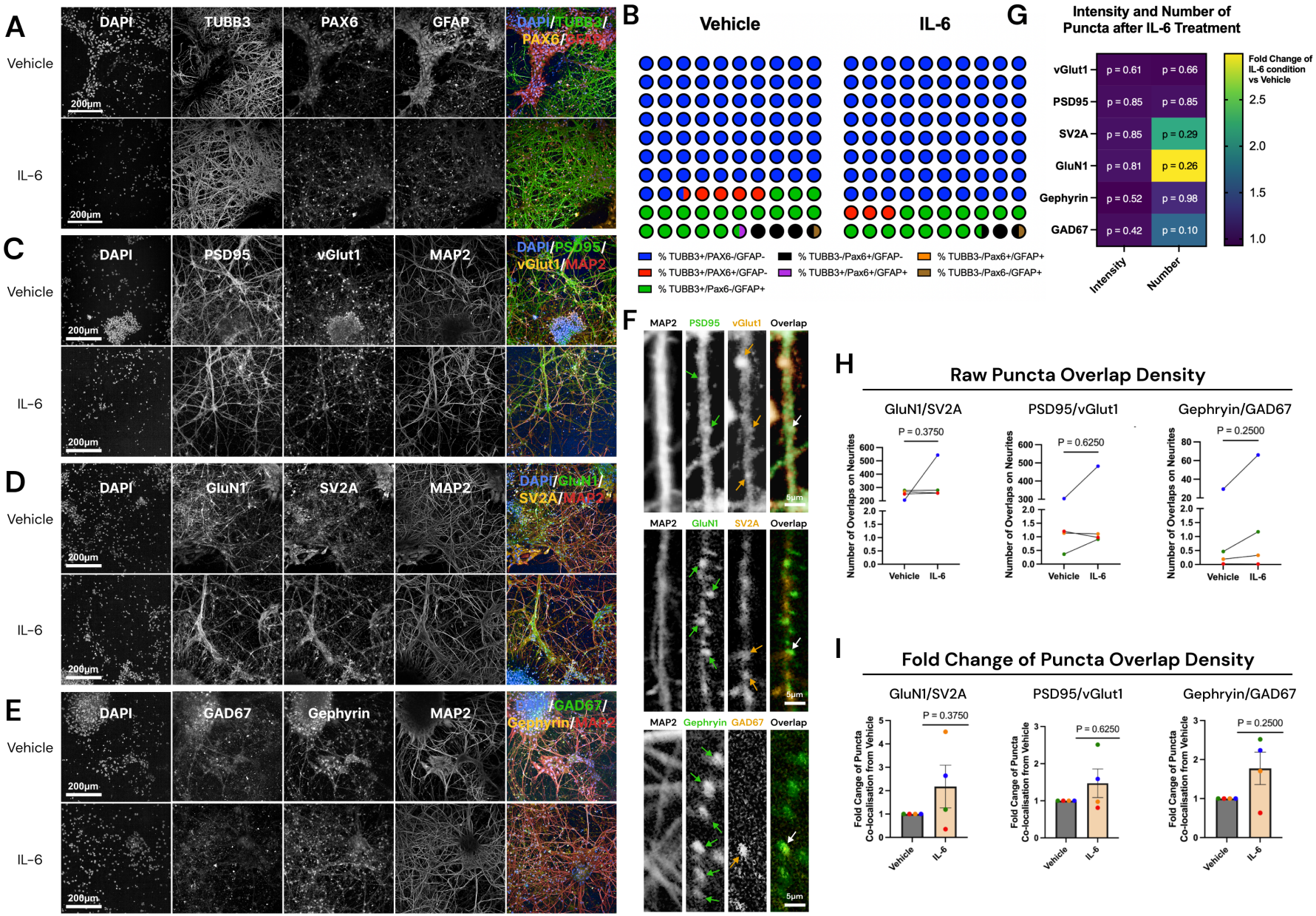
A
Vehicle
IL-6
DAPI
TUBB3
PAX6
GFAP
DAPI/TUBB3/PAX6/GFAP
200µm
B
Vehicle
IL-6
% TUBB3+/PAX6-/GFAP-
% TUBB3+/PAX6+/GFAP-
% TUBB3+/Pax6-/GFAP+
% TUBB3-/Pax6+/GFAP-
% TUBB3+/Pax6+/GFAP+
% TUBB3-/Pax6+/GFAP+
% TUBB3-/Pax6-/GFAP+
G
Intensity and Number of Puncta after IL-6 Treatment
vGlut1 p = 0.61 p = 0.66
PSD95 p = 0.85 p = 0.85
SV2A p = 0.85 p = 0.29
GluN1 p = 0.81 p = 0.26
Gephyrin p = 0.52 p = 0.98
GAD67 p = 0.42 p = 0.10
Intensity
Number
Fold Change of IL-6 condition vs Vehicle
2.5
2.0
1.5
1.0
C
DAPI
PSD95
vGlut1
MAP2
DAPI/PSD95/vGlut1/MAP2
D
GluN1
SV2A
DAPI/GluN1/SV2A/MAP2
E
GAD67
Gephyrin
DAPI/GAD67/Gephyrin/MAP2
F
MAP2
PSD95
vGlut1
Overlap
GluN1
SV2A
Gephyrin
GAD67
5µm
H
Raw Puncta Overlap Density
GluN1/SV2A
PSD95/vGlut1
Gephyrin/GAD67
P = 0.3750
P = 0.6250
P = 0.2500
Number of Overlaps on Neurites
Vehicle
IL-6
I
Fold Change of Puncta Overlap Density
Fold Cange of Puncta Co-localisation from Vehicle

802

803 **Figure 5 -** The Long-Term Effect on Terminal Neuron Differentiation After IL-6 Stimulation of NPC in Co-Culture
804 with MGLs. (A) Representative images of cortical neurons from donor 127_CTM_01, exposed to vehicle or IL-6 in
805 co-culture with MGLs at their NPC stage. Cells were stained for DAPI (column 1), TUBB3 (column 2), PAX6 (column
806 3) and GFAP (column 4). Channels were overlayed in column 5. Scale bar represents 200µm. Images from all four
807 donors are available in Supplementary Figure 10. (B) Cell populations of the post-mitotic differentiated cultures for
808 each treatment condition as a percentage of total number of cells counted averaged across donors (N = 4 donors
809 averaged from N= 4 technical well culture repeats each). For clarity, percentage values were rounded to the nearest
810 0.5%. One circle = 1%, with corresponding percentage values found in supplementary table 9. (C-E)
811 Representative images of cortical neurons from healthy control donor 127_CTM_01, exposed to vehicle or IL-6 in
812 co-culture with MGLs at their NPC stage. Scale bar represents 200µm. (C) Cells were stained for DAPI (column 1),
813 PSD95 (column 2), vGlut1 (column 3) and MAP2 (column 4). (D) Cells were stained for DAPI (column 1), GluN1
814 (column 2), SV2A (column 3) and MAP2 (column 4). (E) Cells were stained for DAPI (column 1), Gephyrin (column
815 2), GAD67 (column 3) and MAP2 (column 4). (F) Representative images of pre- and post-synaptic puncta along
816 MAP2+ neurites from 127_CTM. Green and orange arrows indicate locations where one puncta was counted, an
817 white arrows identify a co-localised puncta count. Scale bar represents 5µm. (G) Heatmap of fold change and p-
818 values from one-sample Wilcoxon tests comparing vehicle (value = 1) and IL-6 treated cultures for signal intensity
819 and number of puncta in MAP2+ neurites imaged in figures C-E. Raw metrics were averaged to give one data point
820 per donor, and then IL-6 treated culture values were calculated as a fold change from each donor's vehicle prior to
821 statistical analysis. (H) Raw density of co-localisation events of puncta pairs (GAD67 with Gephyrin, GluN1 with
822 SV2A and vGlut1 with PSD95). Wilcoxon test p-values labelled on graph compare vehicle and IL-6 treated cultures.
823 Technical replicates were averaged to give one data point per donor. Bar graph plotted as mean with standard
824 deviation (SD) error bars, and points coloured by donor line: red (M3_CTR), blue (127_CTM), green (014_CTM)
825 and orange (069_CTF). (I) Fold-change from vehicle of co-localisation events of puncta pairs (GAD67 with
826 Gephyrin, GluN1 with SV2A and vGlut1 with PSD95). One-sample Wilcoxon test p-values labelled on graph
827 compare vehicle and IL-6 treated cultures. Similarly, metrics were averaged to give one data point per donor and
828 then IL-6 treated culture values were calculated as a fold change from each donor's vehicle. Bar graph plotted as
829 mean with standard deviation (SD) error bars, and points coloured by donor line: red (M3_CTR), blue (127_CTM),
830 green (014_CTM) and orange (069_CTF).

831 ## Discussion

832 Our study aimed to determine the role of prenatal IL-6 signalling and how it might
833 contribute to the risk of psychiatric disorders with a putative neurodevelopmental origin,
834 by particularly focusing on the interactions between forebrain neural progenitor cells
835 and microglia-like cells derived from hiPSCs. Our findings demonstrated that forebrain
836 NPCs in monoculture can respond to IL-6 via trans-signalling in the presence of a
837 recombinant soluble IL-6 receptor by activating the JAK/STAT pathway, and this
838 response is dose-dependent on the soluble receptor concentration. This finding aligns
839 with earlier observation that NPCs do not respond to IL-6 in monoculture in the
840 absence of exogenous IL-6Ra or hyper-IL-6 (Couch *et al.*, 2023; Sarieva, Hildebrand,
841 *et al.*, 2023). We further demonstrated that MGLs secrete soluble IL-6R and other
842 cytokines in response to IL-6, including TNF-alpha, which has been previously
843 identified as a key effector molecule in rodent models of maternal immune activation
844 (Potter 2023). Contrary to our hypothesis, NPCs displayed only a marginal
845 transcriptional response to IL-6 stimulation when in co-culture with MGLs, with only
846 two genes showing differential expression passing the 5% FDR threshold. This finding
847 particularly contrasts the substantial transcriptional changes observed in MGLs,
848 indicating cell-type specific sensitivities to IL-6 signalling, as previously described in
849 mono-culture (Couch *et al.*, 2023). Moreover, concerning the enduring effects of short-
850 term IL-6 exposure during the NPC stage, our findings revealed no marked changes
851 in the differentiation paths of forebrain NPCs into diverse cell types. This contrasts
852 with earlier findings in hiPSC-derived neuronal cultures that cell-fate acquisition is
853 affected by IL-6 (Sarieva, Kagermeier, *et al.*, 2023), but noting that Sarieva at
854 colleagues (2023) stimulated their cultures with hyper-IL-6, driving trans-IL6 signalling,
855 for five days. Furthermore, IL-6 exposure did not significantly affect synaptic densities

856 or intensities in post-mitotic forebrain cortical neurons. Regional or species differences
857 in the effects of IL-6 on synaptogenesis may explain why these data conflict with
858 previous research that suggest early IL-6 exposure has the potential to alter
859 synaptogenesis in the hippocampus of a rodent model (Samuelsson *et al.*, 2006;
860 Mirabella *et al.*, 2021). It is important to emphasise that the findings of our study are
861 of relevance primarily to dorsal and ventral forebrain NPCs. Although this study
862 observed no specific subpopulation of NPCs to respond to IL-6 via cis-signalling, it is
863 possible that NPCs and subsequently differentiating post-mitotic neurons from brain
864 regions other than the developing cortex might respond differently, such as in the
865 hippocampus or the midbrain. For example, recent evidence suggests the
866 immortalised human dopaminergic neuronal precursor cell line LUHMES (Lotharius *et*
867 *al.*, 2002) expresses low levels of IL6R, albeit very low compared to microglia (Nishi
868 *et al.*, 2023). Furthermore, there are several reports in the literature on the effects of
869 MIA in rodent models using TLR3 agonists on midbrain dopamine neuron
870 development *in vivo*, which are associated with behavioural effects and impaired
871 cortical function (Meyer *et al.*, 2008; Vuillermot *et al.*, 2010; Luchicchi *et al.*, 2016;
872 Purves-Tyson *et al.*, 2021; Perez-Palomar *et al.*, 2023). Therefore, we suggest our 2D
873 hiPSC-derived forebrain co-culture model offers a simplistic, reproducible and
874 scalable model that we can use to test hypotheses that NPCs with different regional
875 origins, for example forebrain and midbrain, may show differential responses to IL-6
876 as a result.

877

878 We observe a lack of substantial transcriptional and cellular effects in NPCs co-
879 cultured with MGLs and stimulated with IL-6, despite MGLs secreting the soluble IL-
880 6R and other cytokines. Notably, the sIL-6Ra concentration secreted by MGLs in our

881 study was low (0.29 ng/ml), falling below the concentration necessary to trigger STAT3
882 phosphorylation in NPCs in response to IL-6 and recombinant IL-6Ra (more than
883 1ng/ml required). Furthermore, the concentration of sIL-6Ra in our co-culture system
884 is lower than that reported in human (adult) CSF under both basal and inflammatory
885 disease states, acknowledging that we lack data on sIL-6Ra levels during human
886 development in either state. Hence, there simply may not have been enough sIL-6Ra
887 secreted by the microglia to initiate trans-signalling in the NPCs. These data highlight
888 the importance of considering the overall human-specific cytokine milieu in our *in vitro*
889 model, and while our iterative study initially focuses on IL-6, future research should
890 explore species differences with other cytokines to better understand the MIA impact
891 on foetal cortical development. Whilst mechanistic animal studies confirm that IL-6 is
892 necessary and sufficient for many of the biological effects of maternal immune
893 activation, the involvement of several other cytokines, including IL-1β (Allswede *et al.*,
894 2020), IL-17A (Choi *et al.*, 2016), TNF-α (Allswede *et al.*, 2020; Potter *et al.*, 2023),
895 and IFN-γ (Goines *et al.*, 2011; Warre-Cornish *et al.*, 2020; Bhat *et al.*, 2022), should
896 not be discounted. The co-culture secretome analysis suggested that TNF-α secreted
897 by microglia following stimulation with IL-6 could act as a potential downstream
898 effector in NPCs. This is supported by the knowledge that NPCs possess receptors
899 for TNF-α (*TNFRSS1A/B)* at the relevant differentiation timepoint (Couch *et al.*, 2023),
900 and can respond to this cytokine *in vivo* following maternal immune activation (Potter
901 *et al.*, 2023). Furthermore, the TNF-α family gene *TNFAIP3* was one of only two genes
902 with differentially increased expression in the NPCs after IL-6 exposure and is known
903 for its role in cytokine-mediated immune responses and was previously reported to be
904 upregulated in neural stem cells infected with ZIKA virus (McGrath *et al.*, 2017). The
905 other gene with increased expression in NPCs, *PABPC1,* is involved in ribosomal

906 recruitment and protein synthesis (Kawahara *et al.*, 2008). Apart from TNF-α, the
907 cytokines showing the greatest change in profiler signals following IL-6 stimulation in
908 co-culture were MIP-1α/MIP-1β, RANTES, GROα, and PF4. Yet, RNAseq data from
909 the NPCs reveal that this cell type is not likely to be the target for these cytokines,
910 given they exhibit relatively low expression levels of specific cytokine receptors such
911 as CCR1 and CXCR3 (normalized DESeq2 counts: 1.02 ± 0.05 and 1.85 ± 0.4,
912 respectively) and align with those from previous forebrain transcriptomic sets (Zhang
913 *et al.*, 2016; Nowakowski *et al.*, 2017; Polioudakis *et al.*, 2019). Additionally, co-
914 culturing MGLs with NPCs could induce specific cytokine responses absent in mono-
915 cultures, as VEGF levels have been shown to be higher in co-cultures stimulated with
916 LPS and IFN-γ (Haenseler *et al.*, 2017). Future studies should investigate the impact
917 of NPC and MGL co-culture on secreted factors from both cell types. Overall, these
918 data highlight the significance of incorporating microglia in *in vitro* NDD models, but
919 also cell types in addition to NPCs that can respond to the microglial secretome for a
920 more accurate representation.

921

922 Building on this idea, only MGLs and NPCs were used in the study for simplicity, and
923 the mechanism by which IL-6 confers increased risk for NDDs likely requires additional
924 cell types. Consistent with this view, Campbell et al. (2014) identified cell types in
925 mouse cerebrum and cerebellum that are responsive to IL-6 via trans-signalling, which
926 included GFAP-positive astrocytes, Bergmann glia, lectin-bound microglia, and
927 vascular endothelial cells, with scarce presence of IL-6 trans-signalling in neurons.
928 Combining these rodent findings with our human cellular data suggests that IL-6 trans-
929 signalling to neural progenitor cells and neurons may not be the direct, central
930 pathogenic mechanism in the developing forebrain, cerebellum, and cerebrum of both

species. This highlights the need for a more complex 3D model, incorporating different regional origins and additional relevant cell types, such as astrocytes, to study the effects of IL-6 on developing neurons (Haddick *et al.*, 2017). Moreover, while hiPSCs provide a valuable model for studying human neurodevelopment within a human-relevant context at a molecular scale, they do not fully capture the complex interactions between additional higher-level systems seen in vivo, such as the peripheral immune system, placenta and blood-brain barrier, which would be relevant in the context of this study (Zaretsky *et al.*, 2004; Campbell *et al.*, 2014; Crockett *et al.*, 2021; Li *et al.*, 2021, 2023; Bermick *et al.*, 2023). Species differences are evident in these interactions. Recent data from a mouse MIA model demonstrated that IL-6 does not pass through the placenta from the dams (Bermick *et al.*, 2023), whereas IL-6 has been shown to transfer through a healthy-term human placental perfusion model (Zaretsky *et al.*, 2004). It is more likely that increased maternal prenatal IL-6 triggers a larger pro-inflammatory chain reaction involving multiple cytokines, cell types, and tissues, indirectly increasing IL-6 in the foetal brain (Schaer *et al.*, 2024). This limitation could be addressed by employing a human-relevant, multi-culture configuration, either in microglial-grafted organoids (Fagerlund *et al.*, 2022; Pașca *et al.*, 2022; Zhang *et al.*, 2022; Schafer *et al.*, 2023) or brain-on-a-chip fluidic systems (Liu *et al.*, 2020, 2022; Vila Cuenca *et al.*, 2021; Pașca *et al.*, 2022). These would offer viable methods to examine whether the release of sIL-6Ra, or other cytokines and chemokines from microglia in response to IL-6 can indeed have an impact on the NPC response, via additional cell types.

Third, after only 24h of IL-6 stimulation in co-culture, cytokine secretion by MGLs in response to IL-6 response might have been either too weak or short to activate

956 relevant pathways in NPCs. In addition, MGLs and NPCs were not in physical contact
957 with each other, therefore precluding conclusions regarding the effects of IL-6 that may
958 occur in a physical co-culture system due to cell-to-cell contact. Our trans-well co-
959 culture model was designed to test hypotheses relating to secreted factors from the
960 MGLs and avoid potential confounds related to cell sorting (Cadiz *et al.*, 2022;
961 Akhmetzyanova, Rizvanov and Mukhamedshina, 2024) in identifying transcriptional
962 effects of IL-6 on MGLs and NPCs in this system. The complexity of a chain of
963 signalling pathways from additional cell types or physical cell connections over a more
964 chronic period may be required to provoke an IL-6 effect on NPC development, which
965 our *in vitro* setting may not entirely replicate, but could be addressed with studies using
966 2D and 3D cultures in combination with single-cell sequencing. Furthermore, NPCs
967 underwent passaging following IL-6 exposure, potentially biasing the sample towards
968 healthier NPCs, leaving behind the ones most affected by IL-6. Therefore, it is
969 important to consider that IL-6 exposure may have long-term effects on developing
970 NPCs when in contact with hiPSC-derived MGLs, and not subjected to post-
971 stimulation passaging. As a result, our study suggests that physical 2D culture and a
972 more prolonged cytokine exposure remains important to test in order to induce
973 substantial changes in NPCs, such as the 5-day exposure to brain organoids by
974 Sarieva and colleagues (2023). Such extended exposure and longer-term culture
975 could more closely mimic the physiological conditions of a long-term prenatal infection,
976 potentially offering a more realistic model for studying the effects of maternal immune
977 activation on foetal brain development (Sarieva, Kagermeier, *et al.*, 2023).

978

979 Fourth, the noticeable presence of variation between different donor lines may mask
980 detectable differences at an averaged donor level. Our sample size of N=4 donor lines,

981 although in line with recommendations for the minimum sample size in such
982 experiments (Dutan Polit *et al.*, 2023), coupled with the variability in responses
983 generated by each individual donor may well constrain our ability to detect group-level
984 differences. Additionally, the diversity among our donor samples may be influenced by
985 sex, as illustrated in Figure 3A PCA, where the sole female line (069_CTF) separates
986 from the three male lines along PC1. The inclusion of only one female line however
987 precludes any conclusion with regard to potential differences in the response to IL-6
988 stimulation as a function of chromosomal sex (XX vs. XY). Future studies using
989 equivalent numbers of XX and XY donor lines or designs incorporating isogenic lines
990 with different sex chromosome content will be required to address this question
991 (Waldhorn *et al.*, 2022). Taken together, these overall sources of variation are
992 consistent with the known heterogeneity of outcomes in response to maternal immune
993 activation in humans and in rodent models, and that in most cases there is no negative
994 outcome in the offspring (Meyer, 2019; Mueller *et al.*, 2019). Therefore, the interaction
995 between environment and genetic background needs to be considered, as evidenced
996 by our findings of differential transcriptional response of NPCs from individuals with
997 schizophrenia to IFN-γ stimulation (Bhat *et al.*, 2022). Given the polygenic nature of
998 NDDs and psychiatric disorders, we suggest hiPSC models that retain the genetic
999 background of the donor are ideally placed to test this (Jansen *et al.*, 2020; Singh *et*
1000 *al.*, 2022; Trubetskoy *et al.*, 2022). When conducting studies to examine the roles of
1001 cytokines on human neurodevelopment *in vitro* using healthy donor lines however,
1002 either greater statistical power, or stratification to allow selection of specific individuals
1003 to study are critical factors to consider when designing future studies. As such our data
1004 may be thought of as part of an iterative process to refine the use of hiPSC models to
1005 study how cytokines influence neurodevelopment in health and disease states.

1006

1007 Despite the minimal impact of IL-6 stimulation on NPCs within our co-culture system
1008 there are clear and replicable effects of IL-6 on hiPSC-derived MGLs that are of
1009 relevance and open new avenues for research. For example, data from mice suggests
1010 that MIA accelerates the developmental programming of microglia, impairing their
1011 intended developmental functions (Matcovitch-Natan *et al.*, 2016). Our previous work
1012 demonstrated that the "MIA Poly I:C GD14 P0" module from Matcovitch-Natan et al.
1013 (2016), a microglial gene set from newborn pups exposed to Poly I:C on gestational
1014 day 14, was the most relevant module overlapping with our upregulated gene set in
1015 hiPSC-derived MGL monocultures exposed to IL-6 for 3h (Couch *et al.*, 2023).
1016 Additionally, a recent study that analysed transcriptomes and epigenetic profiles at
1017 various developmental stages in both foetal and postnatal human microglia has
1018 identified IL-6 as ligand of particular significance in predicting the postnatal microglial
1019 transcriptome, indicating that IL-6 may play a role in promoting the development of a
1020 mature, postnatal microglial phenotype (Han *et al.*, 2023). This raises the idea that the
1021 primary mechanism by which IL-6 increases NDD risk prenatally in offspring could be
1022 via the alteration of typical developmental functions of microglia following IL-6
1023 exposure. This guides several important questions unaddressed by the present study;
1024 (1) are the MGLs in this study are responding to IL-6 through cis- or trans-signalling
1025 (2) what causes the functional shift between these two signalling states, and (3)
1026 whether and how this signalling state transition operates in the CNS, all of which need
1027 to be addressed in future studies. Distinguishing these effects can be carried out in
1028 specific studies to block the IL-6 trans-signalling pathway in microglia using a soluble
1029 IL-6ST compound and compare functional outcomes. Overall, these aspects represent
1030 a critical area for further investigation to understand the complex dynamics of

1031 neurodevelopmental changes under maternal immune activation and the influence of
1032 IL-6 on NDD risk.

1033

1034 In conclusion, our findings show that hiPSC-derived NPCs respond by trans-signalling
1035 to IL-6 when sIL-6Ra is present, above a concentration of 1ng/ml, a level not met by
1036 hiPSC-derived MGLs from healthy donors *in vitro* and unchanged by acute IL-6
1037 stimulation. Although these MGLs secrete a wide range of other cytokines and
1038 chemokines including TNF-α in response to IL-6, the proximal transcriptional and
1039 longer-term cellular effects on NPCs were minimal to absent. On the other hand, MGLs
1040 in co-culture showed robust transcriptional responses to IL-6 consistent with our prior
1041 observations and raising interesting new questions. Based on our observations we
1042 suggest that future studies seeking to develop *in vitro* hiPSC models to decipher the
1043 effects of IL-6 on human neurodevelopment should focus on incorporating microglia
1044 into more complex 3D models containing all relevant glial and neuronal cells that may
1045 respond to the microglia secretome. Such experiments should ideally be carried out
1046 on appropriate genetic risk backgrounds such as high polygenic risk for schizophrenia,
1047 which may reveal important disease-relevant mechanisms. Alternatively individual
1048 donors could be selected based on multivariate data from deeply-phenotype birth
1049 cohorts to identify cellular and molecular mechanisms associated with risk or resilience
1050 to IL-6 exposure during neurodevelopment.

1051 Acknowledgements

1052 The authors acknowledge use of King's Computational Research, Engineering and
1053 Technology Environment (CREATE) and are grateful to Dr George Chennell of the
1054 Wohl Cellular Imaging Centre at King’s College London for technical support during

1055 live imaging. ACMC, DPS and ACV acknowledge financial support for this study from
1056 the National Centre for the Replacement, Refinement and Reduction of Animals in
1057 Research (NC/S001506/1). RM and AB are in receipt of the MRC-Sackler Ph.D.
1058 Programme studentship as part of the MRC Centre for Neurodevelopmental Disorders
1059 (Medical Research Council MR/P502108/1). LS is supported by the UK Medical
1060 Research Council (MR/N013700/1) and King's College London member of the MRC
1061 Doctoral Training Partnership in Biomedical Sciences. CR and ACV acknowledge
1062 support by the Neuro-Immune Interactions in Health & Disease Wellcome Trust PhD
1063 Training Programme (218452/Z/19/Z) at King's College London.

1064 **Conflict of Interest**

1065 The authors declare no competing interests.

1066 **References**

1067 Adhya, D. *et al.* (2021) 'Atypical Neurogenesis in Induced Pluripotent Stem Cells From
1068 Autistic Individuals', *Biological Psychiatry*, 89(5), pp. 486–496. doi:
1069 10.1016/j.biopsych.2020.06.014.

1070 Akhmetzyanova, E. R., Rizvanov, A. A. and Mukhamedshina, Y. O. (2024) 'Current
1071 methods for the microglia isolation: Overview and comparative analysis of approaches',
1072 *Cell and Tissue Research*, pp. 147–158. doi: 10.1007/s00441-023-03853-8.

1073 Allswede, D. M. *et al.* (2020) 'Cytokine concentrations throughout pregnancy and risk
1074 for psychosis in adult offspring: a longitudinal case-control study', *The Lancet*
1075 *Psychiatry*, 7(3), pp. 254–261. doi: 10.1016/S2215-0366(20)30006-7.

1076 Arrode-Brusés, G. and Brusés, J. L. (2012) ‘Maternal immune activation by poly(I:C)
1077 induces expression of cytokines IL-1β and IL-13, chemokine MCP-1 and colony
1078 stimulating factor VEGF in fetal mouse brain’, *Journal of Neuroinflammation*, 9. doi:
1079 10.1186/1742-2094-9-83.

1080 Azuma, H. *et al.* (2000) ‘Analysis of soluble interleukin 6 receptor in cerebprospinal
1081 fluid in inflammatory and non-inflammatory conditions’, *Cytokine*, 12(2), pp. 160–164.
1082 doi: 10.1006/cyto.1999.0534.

1083 De Bartolomeis, A. *et al.* (2014) ‘Glutamatergic postsynaptic density protein
1084 dysfunctions in synaptic plasticity and dendritic spines morphology: Relevance to
1085 schizophrenia and other behavioral disorders pathophysiology, and implications for
1086 novel therapeutic approaches’, *Molecular Neurobiology*, pp. 484–511. doi:
1087 10.1007/s12035-013-8534-3.

1088 Bayés, Á. *et al.* (2011) ‘Characterization of the proteome, diseases and evolution of
1089 the human postsynaptic density’, *Nature Neuroscience*, 14(1), pp. 19–21. doi:
1090 10.1038/nn.2719.

1091 Bennett, M. L. *et al.* (2016) ‘New tools for studying microglia in the mouse and human
1092 CNS’, *Proceedings of the National Academy of Sciences of the United States of*
1093 *America*, 113(12), pp. E1738–E1746. doi: 10.1073/pnas.1525528113.

1094 Bermick, J. *et al.* (2023) ‘The fetal response to maternal inflammation is dependent
1095 upon maternal IL-6 in a murine model’, *Cytokine*, 167, p. 156210. doi:
1096 10.1016/j.cyto.2023.156210.

1097 Bhat, A. *et al.* (2022) ‘Attenuated transcriptional response to pro-inflammatory
1098 cytokines in schizophrenia hiPSC-derived neural progenitor cells’, *Brain, Behavior,*
1099 *and Immunity*, 105, pp. 82–97. doi: 10.1016/j.bbi.2022.06.010.

1100 Bitanihirwe, B. K. Y. *et al.* (2009) 'Glutamatergic deficits and parvalbumin-containing
1101 inhibitory neurons in the prefrontal cortex in schizophrenia', *BMC Psychiatry*, 9. doi:
1102 10.1186/1471-244X-9-71.

1103 Cadiz, M. P. *et al.* (2022) 'Culture shock: microglial heterogeneity, activation, and
1104 disrupted single-cell microglial networks in vitro', *Molecular Neurodegeneration*, 17(1).
1105 doi: 10.1186/s13024-022-00531-1.

1106 Campbell, I. L. *et al.* (2014) 'Trans-signaling is a dominant mechanism for the
1107 pathogenic actions of interleukin-6 in the brain', *Journal of Neuroscience*, 34(7), pp.
1108 2503–2513. doi: 10.1523/JNEUROSCI.2830-13.2014.

1109 Chehboun, S. *et al.* (2017) 'Epstein-Barr virus-induced gene 3 (EBI3) can mediate IL-
1110 6 trans-signaling', *Journal of Biological Chemistry*, 292(16), pp. 6644–6656. doi:
1111 10.1074/jbc.M116.762021.

1112 Chesnokov, M. S., Yadav, A. and Chefetz, I. (2022) 'Optimized Transcriptional
1113 Signature for Evaluation of MEK/ERK Pathway Baseline Activity and Long-Term
1114 Modulations in Ovarian Cancer', *International Journal of Molecular Sciences*, 23(21).
1115 doi: 10.3390/ijms232113365.

1116 Choi, G. B. *et al.* (2016) 'The maternal interleukin-17a pathway in mice promotes
1117 autism-like phenotypes in offspring', *Science*, 351(6276), pp. 933–939. doi:
1118 10.1126/science.aad0314.

1119 Chukaew, P. *et al.* (2022) 'Correlation of BDNF, VEGF, TNF-α, and S100B with
1120 cognitive impairments in chronic, medicated schizophrenia patients',
1121 *Neuropsychopharmacology Reports*, 42(3), pp. 281–287. doi: 10.1002/npr2.12261.

1122 Couch, A. C. M. *et al.* (2023) 'Acute IL-6 exposure triggers canonical IL6Ra signaling
1123 in hiPSC microglia, but not neural progenitor cells', *Brain, Behavior, and Immunity*,
1124 110, pp. 43–59. doi: 10.1016/j.bbi.2023.02.007.

1125 Crockett, A. M. *et al.* (2021) 'Disruption of the blood-brain barrier in 22q11.2 deletion
1126 syndrome', *Brain*, 144(5), pp. 1351–1360. doi: 10.1093/brain/awab055.

1127 Deans, P. J. M. *et al.* (2017) 'Psychosis Risk Candidate ZNF804A Localizes to
1128 Synapses and Regulates Neurite Formation and Dendritic Spine Structure', *Biological*
1129 *Psychiatry*, 82(1), pp. 49–61. doi: 10.1016/j.biopsych.2016.08.038.

1130 Dobin, A. *et al.* (2013) 'STAR: Ultrafast universal RNA-seq aligner', *Bioinformatics*,
1131 29(1), pp. 15–21. doi: 10.1093/bioinformatics/bts635.

1132 Dráberová, E. *et al.* (2008) 'Class III β-tubulin is constitutively coexpressed with glial
1133 fibrillary acidic protein and nestin in midgestational human fetal astrocytes:
1134 Implications for phenotypic identity', *Journal of Neuropathology and Experimental*
1135 *Neurology*, 67(4), pp. 341–354. doi: 10.1097/NEN.0b013e31816a686d.

1136 Dutan Polit, L. *et al.* (2023) 'Recommendations, guidelines, and best practice for the
1137 use of human induced pluripotent stem cells for neuropharmacological studies of
1138 neuropsychiatric disorders', *Neuroscience Applied*, 2, p. 101125. doi:
1139 10.1016/J.NSA.2023.101125.

1140 Eze, U. C. *et al.* (2021) 'Single-cell atlas of early human brain development highlights
1141 heterogeneity of human neuroepithelial cells and early radial glia', *Nature*
1142 *Neuroscience*, 24(4), pp. 584–594. doi: 10.1038/s41593-020-00794-1.

1143 Fagerlund, I. *et al.* (2022) 'Microglia-like cells promote neuronal functions in cerebral
1144 organoids', *Cells*, 11(1). doi: 10.3390/cells11010124.

1145 Ferreira, R. C. *et al.* (2013) 'Functional IL6R 358Ala allele impairs classical IL-6
1146 receptor signaling and influences risk of diverse inflammatory diseases', *PLoS*
1147 *genetics*, 9(4). doi: 10.1371/JOURNAL.PGEN.1003444.

1148 Fiebelkow, J. *et al.* (2021) 'The tyrosine phosphatase SHP2 increases robustness and
1149 information transfer within IL-6-induced JAK/STAT signalling', *Cell Communication*
1150 *and Signaling*, 19(1). doi: 10.1186/s12964-021-00770-7.

1151 Florio, M. *et al.* (2015) 'Human-specific gene ARHGAP11B promotes basal progenitor
1152 amplification and neocortex expansion', *Science*, 347(6229), pp. 1465–1470. doi:
1153 10.1126/science.aaa1975.

1154 Glynn, M. W. and McAllister, A. K. (2006) 'Immunocytochemistry and quantification of
1155 protein colocalization in cultured neurons', *Nature Protocols*, 1(3), pp. 1287–1296. doi:
1156 10.1038/nprot.2006.220.

1157 Goines, P. E. *et al.* (2011) 'Increased midgestational IFN-γ, IL-4 and IL-5 in women
1158 bearing a child with autism: A case-control study', *Molecular Autism*, 2(1). doi:
1159 10.1186/2040-2392-2-13.

1160 Graham, A. M. *et al.* (2018) 'Maternal Systemic Interleukin-6 During Pregnancy Is
1161 Associated With Newborn Amygdala Phenotypes and Subsequent Behavior at 2
1162 Years of Age', *Biological Psychiatry*, 83(2), pp. 109–119. doi:
1163 10.1016/j.biopsych.2017.05.027.

1164 Grunwald, L. M. *et al.* (2019) 'Comparative characterization of human induced
1165 pluripotent stem cells (hiPSC) derived from patients with schizophrenia and autism',
1166 *Translational Psychiatry*, 9(1). doi: 10.1038/s41398-019-0517-3.

1167 Guidotti, A. *et al.* (2000) 'Decrease in reelin and glutamic acid decarboxylase67
1168 (GAD67) expression in schizophrenia and bipolar disorder: A postmortem brain study',
1169 *Archives of General Psychiatry*, 57(11), pp. 1061–1069. doi:
1170 10.1001/archpsyc.57.11.1061.

1171 Haddick, P. C. G. *et al.* (2017) 'A Common Variant of IL-6R is Associated with Elevated
1172 IL-6 Pathway Activity in Alzheimer's Disease Brains', *Journal of Alzheimer's Disease*,
1173 56(3), pp. 1037–1054. doi: 10.3233/JAD-160524.

1174 Haenseler, W. *et al.* (2017) 'A Highly Efficient Human Pluripotent Stem Cell Microglia
1175 Model Displays a Neuronal-Co-culture-Specific Expression Profile and Inflammatory
1176 Response', *Stem Cell Reports*, 8(6), pp. 1727–1742. doi:
1177 10.1016/j.stemcr.2017.05.017.

1178 Han, C. Z. *et al.* (2023) 'Human microglia maturation is underpinned by specific gene
1179 regulatory networks', *Immunity*, 56(9), pp. 2152-2171.e13. doi:
1180 10.1016/j.immuni.2023.07.016.

1181 Hashimoto, T. *et al.* (2008) 'Alterations in GABA-related transcriptome in the
1182 dorsolateral prefrontal cortex of subjects with schizophrenia', *Molecular Psychiatry*,
1183 13(2), pp. 147–161. doi: 10.1038/sj.mp.4002011.

1184 Holloway, T. *et al.* (2013) 'Prenatal stress induces schizophrenia-like alterations of
1185 serotonin 2A and metabotropic glutamate 2 receptors in the adult offspring: Role of
1186 maternal immune system', *Journal of Neuroscience*, 33(3), pp. 1088–1098. doi:
1187 10.1523/JNEUROSCI.2331-12.2013.

1188 Jansen, A. G. *et al.* (2020) 'Psychiatric Polygenic Risk Scores as Predictor for
1189 Attention Deficit/Hyperactivity Disorder and Autism Spectrum Disorder in a Clinical

1190 Child and Adolescent Sample', *Behavior Genetics*, 50(4), pp. 203–212. doi:
1191 10.1007/s10519-019-09965-8.

1192 Jao, J. and Ciernia, A. V. (2021) 'MGEnrichment: A web application for microglia gene
1193 list enrichment analysis', *PLoS Computational Biology*, 17(11), p. e1009160. doi:
1194 10.1371/journal.pcbi.1009160.

1195 Karolewicz, B. *et al.* (2010) 'Reduced level of glutamic acid decarboxylase-67 kDa in
1196 the prefrontal cortex in major depression', *International Journal of*
1197 *Neuropsychopharmacology*, 13(4), pp. 411–420. doi: 10.1017/S1461145709990587.

1198 Kawahara, H. *et al.* (2008) 'Neural RNA-binding protein Musashi1 inhibits translation
1199 initiation by competing with eIF4G for PABP', *Journal of Cell Biology*, 181(4), pp. 639–
1200 653. doi: 10.1083/jcb.200708004.

1201 Khandaker, G. M. *et al.* (2014) 'Association of serum interleukin 6 and C-reactive
1202 protein in childhood with depression and psychosis in young adult life a population-
1203 based longitudinal study', *JAMA Psychiatry*, 71(10), pp. 1121–1128. doi:
1204 10.1001/jamapsychiatry.2014.1332.

1205 Kuljis, D. A. *et al.* (2019) 'Fluorescence-based quantitative synapse analysis for cell
1206 type-specific connectomics', *eNeuro*, 6(5). doi: 10.1523/ENEURO.0193-19.2019.

1207 Li, H. *et al.* (2009) 'The Sequence Alignment/Map format and SAMtools',
1208 *Bioinformatics*, 25(16), pp. 2078–2079. doi: 10.1093/bioinformatics/btp352.

1209 Li, Y. *et al.* (2021) 'Investigation of neurodevelopmental deficits of 22 q11.2 deletion
1210 syndrome with a patient-ipsc-derived blood–brain barrier model', *Cells*, 10(10). doi:
1211 10.3390/cells10102576.

1212 Li, Y. *et al.* (2023) 'Inhibition of Abl Kinase by Imatinib Can Rescue the Compromised
1213 Barrier Function of 22q11.2DS Patient-iPSC-Derived Blood–Brain Barriers', *Cells*,
1214 12(3). doi: 10.3390/cells12030422.

1215 Liao, Y. *et al.* (2019) 'WebGestalt 2019: gene set analysis toolkit with revamped UIs
1216 and APIs', *Nucleic Acids Research*, 47(W1), pp. W199–W205. doi:
1217 10.1093/nar/gkz401.

1218 Liao, Y., Smyth, G. K. and Shi, W. (2019) 'The R package Rsubread is easier, faster,
1219 cheaper and better for alignment and quantification of RNA sequencing reads', *Nucleic*
1220 *Acids Research*, 47(8), p. e47. doi: 10.1093/nar/gkz114.

1221 Lionel, A. C. *et al.* (2013) 'Rare exonic deletions implicate the synaptic organizer
1222 gephyrin (GPHN) in risk for autism, schizophrenia and seizures', *Human Molecular*
1223 *Genetics*, 22(10), pp. 2055–2066. doi: 10.1093/hmg/ddt056.

1224 Liu, L. *et al.* (2020) 'Three-dimensional brain-on-chip model using human iPSC-
1225 derived GABAergic neurons and astrocytes: Butyrylcholinesterase posttreatment for
1226 acute malathion exposure', *PLoS ONE*, 15(3). doi: 10.1371/journal.pone.0230335.

1227 Liu, L. *et al.* (2022) 'A Three-Dimensional Brain-on-a-Chip Using Human iPSC-Derived
1228 GABAergic Neurons and Astrocytes', in *Methods in Molecular Biology*, pp. 117–128.
1229 doi: 10.1007/978-1-0716-2289-6_6.

1230 Lotharius, J. *et al.* (2002) 'Effect of mutant α-synuclein on dopamine homeostasis in a
1231 new human mesencephalic cell line', *Journal of Biological Chemistry*, 277(41), pp.
1232 38884–38894. doi: 10.1074/jbc.M205518200.

1233 Love, M. I., Huber, W. and Anders, S. (2014) 'Moderated estimation of fold change
1234 and dispersion for RNA-seq data with DESeq2', *Genome Biology*, 15(12), pp. 1–21.
1235 doi: 10.1186/s13059-014-0550-8.

1236 Luchicchi, A. *et al.* (2016) 'Maternal immune activation disrupts dopamine system in
1237 the offspring', *International Journal of Neuropsychopharmacology*, 19(7), pp. 1–10. doi:
1238 10.1093/ijnp/pyw007.

1239 Matcovitch-Natan, O. *et al.* (2016) 'Microglia development follows a stepwise program
1240 to regulate brain homeostasis', *Science*, 353(6301). doi: 10.1126/science.aad8670.

1241 McGrath, E. L. *et al.* (2017) 'Differential Responses of Human Fetal Brain Neural Stem
1242 Cells to Zika Virus Infection', *Stem Cell Reports*, 8(3), pp. 715–727. doi:
1243 10.1016/j.stemcr.2017.01.008.

1244 Melief, J. *et al.* (2012) 'Phenotyping primary human microglia: Tight regulation of LPS
1245 responsiveness', *GLIA*, 60(10), pp. 1506–1517. doi: 10.1002/glia.22370.

1246 Meyer, U. *et al.* (2008) 'Preliminary evidence for a modulation of fetal dopaminergic
1247 development by maternal immune activation during pregnancy', *Neuroscience*, 154(2),
1248 pp. 701–709. doi: 10.1016/j.neuroscience.2008.04.031.

1249 Meyer, U. (2019) 'Neurodevelopmental Resilience and Susceptibility to Maternal
1250 Immune Activation', *Trends in Neurosciences*, 42(11), pp. 793–806. doi:
1251 10.1016/j.tins.2019.08.001.

1252 Mirabella, F. *et al.* (2021) 'Prenatal interleukin 6 elevation increases glutamatergic
1253 synapse density and disrupts hippocampal connectivity in offspring', *Immunity*, 54(11),
1254 pp. 2611-2631.e8. doi: 10.1016/j.immuni.2021.10.006.

1255 Miyata, S. *et al.* (2021) 'Global knockdown of glutamate decarboxylase 67 elicits
1256 emotional abnormality in mice', *Molecular Brain*, 14(1). doi: 10.1186/s13041-020-
1257 00713-2.

1258 Moghaddam, B. and Javitt, D. (2012) 'From revolution to evolution: The glutamate
1259 hypothesis of schizophrenia and its implication for treatment',
1260 *Neuropsychopharmacology*, 37(1), pp. 4–15. doi: 10.1038/npp.2011.181.

1261 Mueller, F. S. *et al.* (2019) 'Influence of poly(I:C) variability on thermoregulation,
1262 immune responses and pregnancy outcomes in mouse models of maternal immune
1263 activation', *Brain, Behavior, and Immunity*, 80, pp. 406–418. doi:
1264 10.1016/j.bbi.2019.04.019.

1265 Nehme, R. *et al.* (2018) 'Combining NGN2 Programming with Developmental
1266 Patterning Generates Human Excitatory Neurons with NMDAR-Mediated Synaptic
1267 Transmission', *Cell Reports*, 23(8), pp. 2509–2523. doi: 10.1016/j.celrep.2018.04.066.

1268 Nieland, T. J. F. *et al.* (2014) 'High content image analysis identifies novel regulators
1269 of synaptogenesis in a high-throughput RNAi screen of primary neurons', *PLoS ONE*,
1270 9(3), p. 91744. doi: 10.1371/journal.pone.0091744.

1271 Nishi, K. *et al.* (2023) 'IL-6-Mediated Upregulated miRNAs in Extracellular Vesicles
1272 Derived from Lund Human Mesencephalic (LUHMES) Cells: Effects on Astrocytes and
1273 Microglia', *Biomolecules*, 13(5). doi: 10.3390/biom13050718.

1274 Nowakowski, T. J. *et al.* (2017) 'Spatiotemporal gene expression trajectories reveal
1275 developmental hierarchies of the human cortex', *Science*, 358(6368), pp. 1318–1323.
1276 doi: 10.1126/science.aap8809.

1277 Oni-Orisan, A. *et al.* (2008) 'Altered Vesicular Glutamate Transporter Expression in
1278 the Anterior Cingulate Cortex in Schizophrenia', *Biological Psychiatry*, 63(8), pp. 766–
1279 775. doi: 10.1016/j.biopsych.2007.10.020.

1280 Onwordi, E. C. *et al.* (2020) 'Synaptic density marker SV2A is reduced in
1281 schizophrenia patients and unaffected by antipsychotics in rats', *Nature*
1282 *Communications*, 11(1), pp. 1–11. doi: 10.1038/s41467-019-14122-0.

1283 Onwordi, E. C. *et al.* (2023) 'Synaptic Terminal Density Early in the Course of
1284 Schizophrenia: An In Vivo UCB-J Positron Emission Tomographic Imaging Study of
1285 Synaptic Vesicle Glycoprotein 2A', *Biological Psychiatry*, 0(0). doi:
1286 10.1016/j.biopsych.2023.05.022.

1287 Ozaki, K. *et al.* (2020) 'Maternal immune activation induces sustained changes in fetal
1288 microglia motility', *Scientific Reports*, 10(1), pp. 1–19. doi: 10.1038/s41598-020-
1289 78294-2.

1290 Pantazis, C. B. *et al.* (2022) 'A reference human induced pluripotent stem cell line for
1291 large-scale collaborative studies', *Cell Stem Cell*, 29(12), pp. 1685-1702.e22. doi:
1292 10.1016/j.stem.2022.11.004.

1293 Park, G. H. *et al.* (2020) 'Activated microglia cause metabolic disruptions in
1294 developmental cortical interneurons that persist in interneurons from individuals with
1295 schizophrenia', *Nature Neuroscience*, 23(11), pp. 1352–1364. doi: 10.1038/s41593-
1296 020-00724-1.

1297 Pașca, S. P. *et al.* (2022) 'A nomenclature consensus for nervous system organoids
1298 and assembloids', *Nature*, 609(7929), pp. 907–910. doi: 10.1038/s41586-022-05219-
1299 6.

1300 Perez-Palomar, B. *et al.* (2023) 'Maternal Immune Activation Induces Cortical
1301 Catecholaminergic Hypofunction and Cognitive Impairments in Offspring', *Journal of*
1302 *Neuroimmune Pharmacology*, 18(3), pp. 348–365. doi: 10.1007/s11481-023-10070-1.

1303 Polioudakis, D. *et al.* (2019) 'A Single-Cell Transcriptomic Atlas of Human Neocortical
1304 Development during Mid-gestation', *Neuron*, 103(5), pp. 785-801.e8. doi:
1305 10.1016/j.neuron.2019.06.011.

1306 Potter, H. G. *et al.* (2023) 'Maternal behaviours and adult offspring behavioural deficits
1307 are predicted by maternal TNFα concentration in a rat model of neurodevelopmental
1308 disorders', *Brain, Behavior, and Immunity*, 108, pp. 162–175. doi:
1309 10.1016/J.BBI.2022.12.003.

1310 Purves-Tyson, T. D. *et al.* (2021) 'Increased levels of midbrain immune-related
1311 transcripts in schizophrenia and in murine offspring after maternal immune activation',
1312 *Molecular Psychiatry*, 26(3), pp. 849–863. doi: 10.1038/s41380-019-0434-0.

1313 Rasmussen, J. M. *et al.* (2019) 'Maternal Interleukin-6 concentration during pregnancy
1314 is associated with variation in frontolimbic white matter and cognitive development in
1315 early life', *NeuroImage*, 185, pp. 825–835. doi: 10.1016/j.neuroimage.2018.04.020.

1316 Reeh, H. *et al.* (2019) 'Response to IL-6 trans- A nd IL-6 classic signalling is
1317 determined by the ratio of the IL-6 receptor α to gp130 expression: Fusing
1318 experimental insights and dynamic modelling', *Cell Communication and Signaling*,
1319 17(1), pp. 1–21. doi: 10.1186/s12964-019-0356-0.

1320 Rose-John, S. (2001) 'Coordination of interleukin-6 biology by membrane bound and
1321 soluble receptors', in *Advances in Experimental Medicine and Biology*. Kluwer
1322 Academic/Plenum Publishers, pp. 145–151. doi: 10.1007/978-1-4615-0685-0_19.

1323 Rose-John, S. *et al.* (2009) 'Interleukin-6 Trans-Signaling and Colonic Cancer
1324 Associated with Inflammatory Bowel Disease', *Current Pharmaceutical Design*, 15(18),
1325 pp. 2095–2103. doi: 10.2174/138161209788489140.

1326 Rose-John, S. (2012) 'Il-6 trans-signaling via the soluble IL-6 receptor: Importance for
1327 the proinflammatory activities of IL-6', *International Journal of Biological Sciences*, 8(9),
1328 pp. 1237–1247. doi: 10.7150/ijbs.4989.

1329 Rose-John, S. (2018) 'Interleukin-6 family cytokines', *Cold Spring Harbor Perspectives*
1330 *in Biology*, 10(2). doi: 10.1101/cshperspect.a028415.

1331 Rudolph, M. D. *et al.* (2018) 'Maternal IL-6 during pregnancy can be estimated from
1332 newborn brain connectivity and predicts future working memory in offspring', *Nature*
1333 *Neuroscience*, 21(5), pp. 765–772. doi: 10.1038/s41593-018-0128-y.

1334 Samuelsson, A. M. *et al.* (2006) 'Prenatal exposure to interleukin-6 results in
1335 inflammatory neurodegeneration in hippocampus with NMDA/GABAA dysregulation
1336 and impaired spatial learning', *American Journal of Physiology - Regulatory Integrative*
1337 *and Comparative Physiology*, 290(5), pp. 1345–1356. doi:
1338 10.1152/ajpregu.00268.2005.

1339 Sarieva, K., Kagermeier, T., *et al.* (2023) 'Human brain organoid model of maternal
1340 immune activation identifies radial glia cells as selectively vulnerable', *Molecular*
1341 *Psychiatry*, pp. 1–13. doi: 10.1038/s41380-023-01997-1.

1342 Sarieva, K., Hildebrand, F., *et al.* (2023) 'Pluripotent stem cell-derived neural
1343 progenitor cells can be used to model effects of IL-6 on human neurodevelopment',
1344 *Disease Models & Mechanisms*, 16(11). doi: 10.1242/DMM.050306.

1345 Schaer, R. *et al.* (2024) 'Intrauterine position effects in a mouse model of maternal
1346 immune activation', *Brain, Behavior, and Immunity*, 120, pp. 391–402.

1347 Schafer, S. T. *et al.* (2023) 'An in vivo neuroimmune organoid model to study human
1348 microglia phenotypes', *Cell*, 186(10), pp. 2111-2126.e20. doi:
1349 10.1016/J.CELL.2023.04.022.

1350 Scheller, J. *et al.* (2011) 'The pro- and anti-inflammatory properties of the cytokine
1351 interleukin-6', *Biochimica et Biophysica Acta - Molecular Cell Research*, 1813(5), pp.
1352 878–888. doi: 10.1016/j.bbamcr.2011.01.034.

1353 Shi, Y., Kirwan, P. and Livesey, F. J. (2012) 'Directed differentiation of human
1354 pluripotent stem cells to cerebral cortex neurons and neural networks', *Nature*
1355 *Protocols*, 7(10), pp. 1836–1846. doi: 10.1038/nprot.2012.116.

1356 Shum, C. *et al.* (2015) 'Utilizing induced pluripotent stem cells (iPSCs) to understand
1357 the actions of estrogens in human neurons', *Hormones and Behavior*, 74, pp. 228–
1358 242. doi: 10.1016/j.yhbeh.2015.06.014.

1359 Shum, C. *et al.* (2020) 'Δ9-tetrahydrocannabinol and 2-AG decreases neurite
1360 outgrowth and differentially affects ERK1/2 and Akt signaling in hiPSC-derived cortical
1361 neurons', *Molecular and Cellular Neuroscience*, 103. doi: 10.1016/j.mcn.2019.103463.

1362 Singh, T. *et al.* (2022) 'Rare coding variants in ten genes confer substantial risk for
1363 schizophrenia', *Nature*, 604(7906), pp. 509–516. doi: 10.1038/s41586-022-04556-w.

1364 Smith, S. E. P. *et al.* (2007) 'Maternal immune activation alters fetal brain development
1365 through interleukin-6', *Journal of Neuroscience*, 27(40), pp. 10695–10702. doi:
1366 10.1523/JNEUROSCI.2178-07.2007.

1367 Südhof, T. C. (2017) ‘Synaptic Neurexin Complexes: A Molecular Code for the Logic
1368 of Neural Circuits’, *Cell*. Cell, pp. 745–769. doi: 10.1016/j.cell.2017.10.024.

1369 Trubetskoy, V. *et al.* (2022) ‘Mapping genomic loci implicates genes and synaptic
1370 biology in schizophrenia’, *Nature 2022 604:7906*, 604(7906), pp. 502–508. doi:
1371 10.1038/s41586-022-04434-5.

1372 Vila Cuenca, M. *et al.* (2021) ‘Engineered 3D vessel-on-chip using hiPSC-derived
1373 endothelial- and vascular smooth muscle cells’, *Stem Cell Reports*, 16(9), pp. 2159–
1374 2168. doi: 10.1016/j.stemcr.2021.08.003.

1375 Vuillermot, S. *et al.* (2010) ‘A longitudinal examination of the neurodevelopmental
1376 impact of prenatal immune activation in mice reveals primary defects in dopaminergic
1377 development relevant to schizophrenia’, *Journal of Neuroscience*, 30(4), pp. 1270–
1378 1287. doi: 10.1523/JNEUROSCI.5408-09.2010.

1379 Waldhorn, I. *et al.* (2022) ‘Modeling sex differences in humans using isogenic induced
1380 pluripotent stem cells’, *Stem Cell Reports*, 17(12), pp. 2732–2744. doi:
1381 10.1016/j.stemcr.2022.10.017.

1382 Warre-Cornish, K. *et al.* (2020) ‘Interferon-γ signaling in human iPSC–derived neurons
1383 recapitulates neurodevelopmental disorder phenotypes’, *Science Advances*, 6(34).
1384 doi: 10.1126/sciadv.aay9506.

1385 van Wilgenburg, B. *et al.* (2013) ‘Efficient, Long Term Production of Monocyte-Derived
1386 Macrophages from Human Pluripotent Stem Cells under Partly-Defined and Fully-
1387 Defined Conditions’, *PLoS ONE*, 8(8). doi: 10.1371/journal.pone.0071098.

Wingett, S. W. and Andrews, S. (2018) ‘FastQ Screen: A tool for multi-genome mapping and quality control’, *F1000Research*, 7, p. 1338. doi: 10.12688/f1000research.15931.2.

Wolf, J., Rose-John, S. and Garbers, C. (2014) ‘Interleukin-6 and its receptors: a highly regulated and dynamic system’, *Cytokine*, 70(1), pp. 11–20. doi: 10.1016/j.cyto.2014.05.024.

Zaretsky, M. V. *et al.* (2004) ‘Transfer of inflammatory cytokines across the placenta’, *Obstetrics and Gynecology*, 103(3). doi: 10.1097/01.AOG.0000114980.40445.83.

Zhang, W. *et al.* (2022) ‘Microglia-containing human brain organoids for the study of brain development and pathology’, *Molecular Psychiatry*, pp. 1–12. doi: 10.1038/s41380-022-01892-1.

Zhang, Y. *et al.* (2016) ‘Purification and Characterization of Progenitor and Mature Human Astrocytes Reveals Transcriptional and Functional Differences with Mouse’, *Neuron*, 89(1), pp. 37–53. doi: 10.1016/j.neuron.2015.11.013.